Crosstalk between AML and stromal cells triggers acetate secretion through the metabolic rewiring of stromal cells

Nuria Vilaplana-Lopera[1], Ruba Almaghrabi[1*], Grigorios Papatzikas[1*], Vincent Cuminetti[2*], Mark Jeeves[1], Elena González[1], Alan Cunningham[3], Ayşegül Erdem[3], Frank Schnuetgen[4,5,6], Manoj Raghavan[1,7], Sandeep Potluri[1,7], Jean-Baptiste Cazier[1], Jan Jacob Schuringa[3], Michelle AC Reed[1], Lorena Arranz[2], Ulrich L Günther[1,8†] and Paloma Garcia[1,9†],

[1] Institute of Cancer and Genomic Sciences, University of Birmingham, Birmingham B15 2TT, United Kingdom
[2] Stem Cells, Ageing and Cancer Research Group, Department of Medical Biology, Faculty of Health Sciences, UiT – The Arctic University of Norway, 9019 Tromsø, Norway
[3] Department of Experimental Hematology, University Medical Center Groningen, University of Groningen, Hanzeplein 1, 9700 RB, Groningen, The Netherlands.
[4] Department of Medicine, Hematology/Oncology, University Hospital Frankfurt, Goethe-University, 60590 Frankfurt, Germany.
[5] Frankfurt Cancer Institute, Goethe-University Frankfurt, 60596 Frankfurt, Germany.
[6] German Cancer Consortium (DKTK), partner site Frankfurt/Mainz, and German Cancer Research Center (DKFZ), Heidelberg, Germany
[7] Centre for Clinical Haematology, University Hospitals Birmingham NHS Foundation Trust, Queen Elizabeth Hospital, Queen Elizabeth Medical Centre, Birmingham, United Kingdom.
[8] Institute of Chemistry and Metabolomics, University of Lübeck, 23562 Lübeck, Germany
[9] Corresponding author
[*] These authors contributed equally
[†] These two authors are co-senior authors.

Acute myeloid leukaemia (AML) cells interact and modulate components of their surrounding microenvironment into their own benefit. Stromal cells have been shown to support AML survival and progression through various mechanisms. Nonetheless, it is unclear whether AML cells could establish beneficial metabolic interactions with stromal cells. Here, we identify a novel metabolic crosstalk between AML and stromal cells where AML cells prompt stromal cells to secrete acetate for their own consumption to feed the tricarboxylic acid cycle (TCA). By performing transcriptome analysis, tracer-based metabolic NMR analysis and ROS measurements, we observe that stromal cells present a higher rate of glycolysis. We also find that acetate in stromal cells is derived from pyruvate via chemical conversion under the influence of reactive oxygen species (ROS) following ROS transfer from AML to stromal cells via gap junctions. Overall, we present a unique metabolic communication between AML and stromal cells that could potentially be exploited for adjuvant therapy.

Keywords: Leukaemic niche, acetate, AML, tracer-based NMR, metabolic crosstalk, ROS, acetate metabolism, gap junctions

Introduction

Acute myeloid leukaemia (AML) is a heterogeneous clonal disease characterised by a rapid proliferation of aberrant immature myeloid cells that accumulate in the bone marrow, and eventually in the blood and other organs, severely impairing normal haematopoiesis. AML cells show a highly adaptive metabolism that allows them to efficiently use a variety of nutrients to obtain energy and generate biomass (reviewed in [1]). This high metabolic plasticity confers AML cells a strong advantage against normal haematopoietic cells and has been related to AML aggressiveness. Although the metabolism in AML cells has been broadly investigated [1], fewer studies have focused on identifying metabolic alterations related to the interaction between AML and niche cells. For instance, AML cells are known to interact and modulate niche components for their own support by secreting soluble factors [2-6], via exosomes [7-9] or by establishing direct interactions, mediated by gap junctions [10] or tunnelling nanotubes [11]. These interactions with components of the niche provide AML cells with survival cues, chemoresistance and increased relapse in AML patients [2,4,7,10,12-14]. Furthermore, it has been reported that adipocytes in the niche secrete fatty acids, which are metabolised by AML cells through β-oxidation to obtain energy, protecting AML cells from apoptosis and ROS [15,16].

As a consequence of their highly proliferative demand, leukaemic stem cells (LSCs) [17-20] and, particularly, chemotherapy-resistant AML cells [21] present abnormally high levels of reactive oxygen species (ROS) [22,23]. How AML cells cope with high ROS levels has been intriguing and recent reports are shedding some light on whether the microenvironment plays a role in the redox metabolism of AML cells. For instance, it was reported that Nestin^{+} bone marrow mesenchymal stem cells (BMSCs) support AML progression by increasing the bioenergetic capacity of AML cells and providing them with glutathione (GSH)-mediated antioxidant defence to balance the excess ROS [14]. Similarly, a recent study showed that co-culturing BMSCs with AML cells leads to a decrease in AML ROS levels due to an activation of the antioxidant enzyme GPx-3 in AML cells [24].

Our work provides new insight into the metabolic and redox crosstalk between AML and stromal cells, revealing a new metabolic interaction between AML and stromal cells. By combining transcriptomic and nuclear magnetic resonance (NMR) data, our results demonstrate that stromal cell metabolism is rewired in co-culture giving higher glycolysis and pyruvate decarboxylation, leading to acetate secretion. Our results also show that AML cells are able to transfer ROS to stromal cells by direct interaction through gap junctions and that these ROS can be used by stromal cells to generate and secrete acetate, which is utilised by AML cells as a biofuel by metabolising it via the

72 TCA cycle. Targeting ROS transfer via modulation of gap junctions to suppress the antioxidant
73 protection provided by stromal cells could serve as an adjuvant therapy to eradicate AML.

Results

Co-culturing AML and stromal cells in direct contact triggers acetate secretion by stromal cells

We first sought to determine whether interactions between AML and stromal cells in co-culture would result in differences in the consumption or production of extracellular metabolites. For this purpose, three AML cell lines (SKM-1, Kasumi-1 and HL-60) were cultured separately and in co-culture with MS-5, a stromal cell line capable of maintaining hematopoiesis [25], and the metabolic composition of the extracellular medium was analysed by ^{1}H-NMR and compared at different time points. The most striking difference found in co-culture compared to cells cultured separately was an increased secretion of acetate, which was common for the three cell lines used (Fig. 1a,b). Moreover, only stromal cells secreted acetate to a lower extent when cultured alone whereas AML cells did not secrete any acetate when cultured alone. Altogether, these findings suggest that acetate secretion is indeed a result of a direct interaction between AML and stromal cells. In addition, the observation that only stromal cells secrete acetate under these conditions suggests that stromal cells could be responsible for the increased acetate secretion found in co-culture.

Moreover, we examined the levels of other common extracellular metabolites, including glucose, lactate, glutamate and glutamine. As shown in Supplementary Fig. 1a higher consumption of glucose along with a higher secretion of lactate was observed in AML and stromal cells in co-culture compared to single cultures, suggesting a higher glycolytic flux in co-culture. However, the levels of glucose consumption and lactate production in co-culture were similar to the sum of the glucose consumption and lactate production levels of the AML and stromal cells in single cultures, suggesting that the overall increase in glycolysis in co-culture was just a result of culturing both cell types together. Additionally, we observed no variation in glutamate and glutamine levels suggesting that these metabolites are not involved in interactions that result from co-culture and are utilised depending on their availability.

The metabolic differences found in co-culture, could be due to altered proliferation under these conditions. To determine whether this was the case, a CFSE-based proliferation assay was performed in which AML cells and not stromal cells were stained and their growth was compared when cultured separately vs in co-culture. Over 48 hours, none of the AML cell lines tested presented differences in their proliferation rates (Supplementary Fig. 2a), thus confirming that the metabolic changes found in co-culture were caused by a mechanism independent from changes in proliferation.

Next, we aimed to determine whether cell-to-cell contact could play a role in the increased acetate secretion found in co-culture. For this we co-cultured AML and stromal cells separated by a permeable membrane, allowing cells to share the extracellular medium but impeding cell-to-cell

107 contact. Co-culturing cells using a permeable membrane blocked the increase in acetate secretion
108 observed under direct contact conditions (Fig. 1c). In fact, cells in co-culture presented lower levels
109 of acetate than MS-5 cells cultured alone revealing that direct cell-to-cell contact is required for
110 acetate secretion in co-culture.

111 To examine whether increased acetate secretion is specific for the interaction of AML cells with
112 stromal cells, we co-cultured AML cells with the cervical cancer cell line HeLa and compared the
113 levels of acetate of each cell type cultured alone. We found that there was no acetate secretion in
114 co-culture, also not by HeLa and AML cells cultured alone (Supplementary Fig. 2b), suggesting that
115 increased acetate secretion could be specific for the AML-stromal interaction.

116 Considering that our previous data seemed to indicate that MS-5 cells were responsible for acetate
117 secretion when co-cultured with AML cell lines, we decided to investigate how the levels of
118 extracellular acetate would vary after separating cells from co-culture. The three AML cell lines were
119 co-cultured for 24h with MS-5 cells prior to separation and were subsequently cultured in the same
120 spent media. Extracellular acetate levels in previously co-cultured MS-5 cells followed a similar trend
121 as before separation, suggesting that it is most likely that MS-5 cells are responsible for the
122 increased acetate secretion found in co-culture (Fig. 1d). Moreover, AML cells did not follow this
123 trend as they either maintained the levels of acetate seen prior to separating the cells (Kasumi-1 and
124 HL-60) or presented only a moderate increase (SKM-1) after being separated from co-culture.

125 We further investigated whether increased acetate secretion could take place in primary co-cultures
126 using AML cells derived from patients and whether acetate secretion in co-culture could be specific
127 for AML cells. To address this question, we isolated the $CD34^+$ population of four primary AML
128 patient samples, and three independent healthy donors, cultured them alone vs in co-culture with
129 MS-5 cells, and analysed the composition of the extracellular medium at different time points. We
130 found that three out of four primary AML samples presented higher levels of acetate when co-
131 cultured with MS-5 cells compared to both MS-5 and AML cells cultured alone (Fig. 1e). Contrary,
132 none of the healthy donor samples showed an increased acetate secretion in co-culture suggesting
133 that acetate secretion is specific for AML cells in co-culture (Fig. 1f).

134 Moreover, we sought to determine whether in an *in vivo* setting, increased acetate production
135 would be observed. For this, acetate levels were analysed in the bone marrow extracellular fluid
136 (BMEF) of mice transplanted either with MLL-AF9 leukaemic cells or with healthy wild type
137 hematopoietic cells. These experiments revealed that a significantly higher amounts of acetate was
138 present in the BMEF of mice suffering from leukaemia compared to controls (Fig. 1g).

139

1

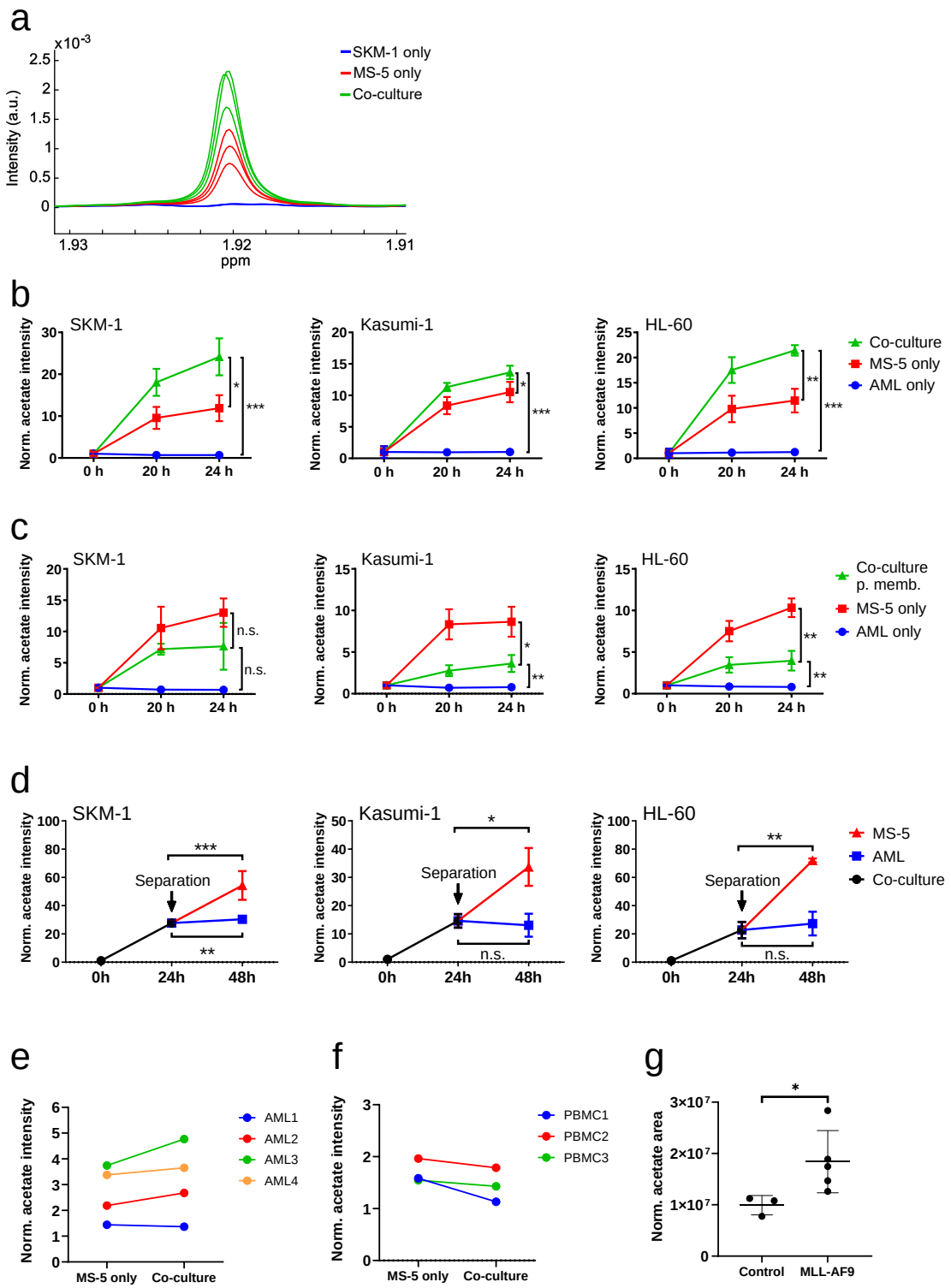
a
x10-3
Intensity (a.u.)
SKM-1 only
MS-5 only
Co-culture
ppm
b
SKM-1
Kasumi-1
HL-60
Norm. acetate intensity
0 h
20 h
24 h
Co-culture
MS-5 only
AML only
c
Co-culture p. memb.
n.s.
d
Separation
0h
24h
48h
MS-5
AML
e
AML1
AML2
AML3
AML4
MS-5 only
Co-culture
f
PBMC1
PBMC2
PBMC3
g
Norm. acetate area
Control
MLL-AF9

140

141

142 **Fig 1. Acetate secretion by stromal cells increases in AML-stroma co-cultures of several**
143 **AML cell lines and primary AML cells in direct contact. a,** Section of ^{1}H-NMR spectra,
144 corresponding to the methyl group of acetate, from extracellular medium samples of SKM-1 cells
145 cultured alone (blue), MS-5 cells cultured alone (red) and SKM-1 and MS-5 cells in co-culture (green)
146 after 24 hours. **b,** Extracellular acetate levels in AML cell lines (SKM-1, Kasumi-1 and HL-60) cultured
147 alone (blue), MS-5 cells cultured alone (red) and AML and MS-5 cells in co-culture in direct contact
148 (green) at 0, 20 and 24 hours of incubation. Each point represents the mean of n=3 independent
149 experiments and error bars represent standard deviations. **c,** Extracellular acetate levels in AML cell
150 lines cultured alone (blue), MS-5 cells cultured alone (red) and AML and MS-5 cells in co-culture
151 separated by a 0.4 µm permeable membrane (green) at 0, 20 and 24 hours of incubation. Each point
152 represents the mean of n=3 independent experiments and error bars represent standard deviations.
153 **d,** Extracellular acetate levels in AML cell lines and MS-5 cells in co-culture (black) for 24 hours and
154 after being separated and cultured alone in the same medium until 48 hours (blue for AML and red
155 for MS-5). Each point represents the mean of n=3 independent experiments and error bars
156 represent standard deviations. **e,** Extracellular acetate levels in MS-5 cells cultured alone (black) and
157 primary patient-derived AML cells co-cultured with MS-5 cells (grey) at 48h. Each set of points
158 represents an independent experiment (n=4). **f,** Extracellular acetate levels in MS-5 cells cultured
159 alone (black) and healthy donor-derived peripheral blood mononuclear $CD34^{+}$ (PBMC) cells co-
160 cultured with MS-5 cells (grey) at 48h. Each set of points represents an independent experiment
161 (n=3). **g**, Acetate levels in bone marrow extracellular fluid of C57BL6/J mice 6 months after
162 transplantation with bone marrow nucleated cells isolated from control or MLL-AF9 transgenic mice.
163 For **b**, **c, d** and **g** unpaired Student's t-tests were applied for each condition (black brackets) and p-
164 values are represented by n.s. for not significant * for p-value<0.05, ** for p-value<0.01 and *** for
165 p-value<0.001.

166

167 **AML cells consume and use acetate secreted by stromal cells to feed the TCA cycle**

168 Following the finding that stromal cells are responsible for acetate secretion in co-culture, we
169 decided to determine whether AML cells might be able to metabolise the secreted acetate. We first
170 sought to define the concentration of secreted acetate in the extracellular medium in co-culture. For
171 this, we compared a sample of extracellular medium from a co-culture of SKM-1 and MS-5 cells after
172 24 hours to a calibration curve (Supplementary Fig. 2c) which allowed us to determine that the
173 concentration of acetate in co-culture, which was approximately of 3 mM. We then investigated
174 whether SKM-1 cells can consume acetate both in physiological and co-culture concentrations. In
175 both cases SKM-1 cells consumed acetate after 48 hours, and in physiological conditions also after
176 24 hours (Fig. 2a).

177 We used a tracer-based approach using [2-^{13}C]acetate to assess whether SKM-1 or MS-5 cells can
178 utilise acetate (Fig. 2b,c and Supplementary Fig. 3a). Both cell types import ^{13}C labelled acetate as
179 observed in NMR spectra (Fig. 2c). However, only SKM-1 cells showed ^{13}C label incorporation in
180 several TCA cycle related metabolites, including aspartate, citrate, glutamate, 2-oxoglutarate,
181 glutathione and proline, as well as in acetylcarnitine. Acetylcarnitine is known to be produced by
182 cells when large amounts of acetyl-CoA are present in the mitochondria [26,27], which could be in line
183 with this experiment in which a 4 mM concentration of [2-^{13}C]acetate was used. Overall, this data
184 suggests that acetate in co-culture could be utilised by SKM-1 cells but not by MS-5 cells.

185 In order to determine whether AML cells can import and metabolise the secreted acetate in co-
186 culture, we co-cultured AML and MS-5 cells for 24 hours, we then added [2-^{13}C]acetate to the spent
187 extracellular medium and cultured cells for 8 hours before analysing the intracellular metabolites in
188 each cell type (Fig. 2d). We found that only AML cells presented ^{13}C labelling in intracellular
189 metabolites (Fig. 2e, Supplementary Fig. 3b). Moreover, the metabolisation pattern for all AML cells
190 was similar to that observed for SKM-1 cells alone (Fig. 2c), where label was incorporated into TCA
191 cycle-related metabolites. Overall, these results revealed that AML cells uptake and utilise the
192 acetate secreted by stromal cells in co-culture as a substrate to feed into the TCA cycle.

193

2

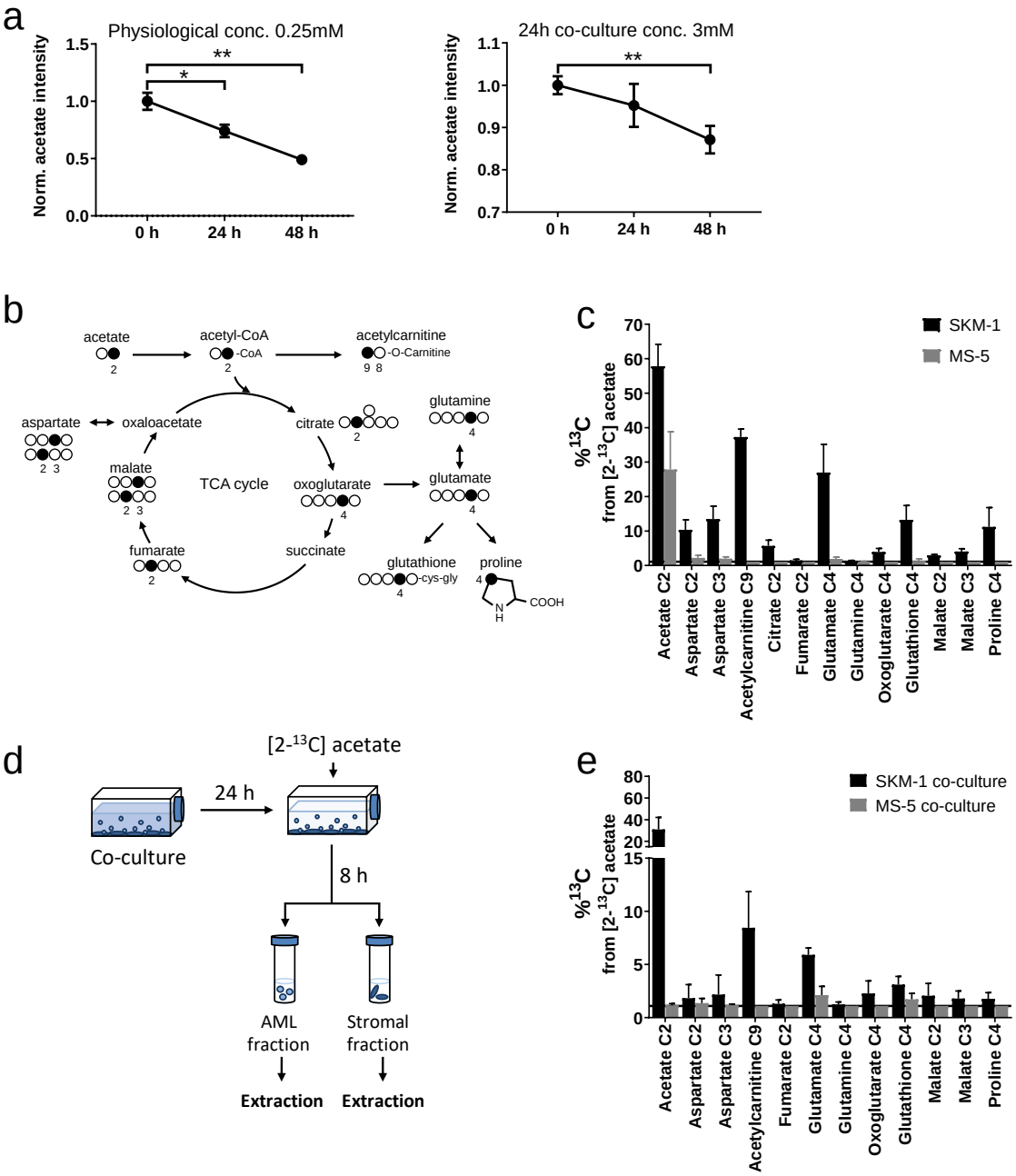
a
Physiological conc. 0.25mM
Norm. acetate intensity
1.5
1.0
0.5
0.0
**
*
0 h
24 h
48 h
24h co-culture conc. 3mM
Norm. acetate intensity
1.1
1.0
0.9
0.8
0.7
**
0 h
24 h
48 h
b
acetate
acetyl-CoA
-CoA
acetylcarnitine
-O-Carnitine
aspartate
oxaloacetate
citrate
glutamine
malate
TCA cycle
oxoglutarate
glutamate
fumarate
succinate
glutathione
-cys-gly
proline
COOH
c
SKM-1
MS-5
%13C
from [2-13C] acetate
Acetate C2
Aspartate C2
Aspartate C3
Acetylcarnitine C9
Citrate C2
Fumarate C2
Glutamate C4
Glutamine C4
Oxoglutarate C4
Glutathione C4
Malate C2
Malate C3
Proline C4
d
[2-13C] acetate
24 h
Co-culture
8 h
AML fraction
Stromal fraction
Extraction
Extraction
e
SKM-1 co-culture
MS-5 co-culture
%13C
from [2-13C] acetate
Acetate C2
Aspartate C2
Aspartate C3
Acetylcarnitine C9
Fumarate C2
Glutamate C4
Glutamine C4
Oxoglutarate C4
Glutathione C4
Malate C2
Malate C3
Proline C4

194

195

196 **Fig. 2. AML cells import the secreted acetate in co-culture to use it as a biofuel. a,**
197 Extracellular acetate levels in SKM-1 cells cultured with 0.25 mM and 3 mM acetate medium after 0,
198 24 and 48 hours. Each point represents the mean of n=3 independent experiments and error bars
199 represent standard deviation. An unpaired Student's t-test was applied for each condition (black
200 brackets) and p-values are represented by * for p-value<0.05, ** for p-value<0.01 and *** for p-
201 value<0.001. **b,** Scheme of label distribution arising from [2-^{13}C]acetate in TCA cycle intermediates.
202 Black circles correspond to expected labelled positions. **c,** ^{13}C percentages of label incorporation in
203 polar metabolites from labelled acetate in SKM-1 and MS-5 cells after two hours of incubation with
204 [2-^{13}C]acetate (4 mM) derived from ^{1}H-^{13}C-HSQC NMR spectra. Bars represent the mean of the ^{13}C
205 percentage and error bars represent the standard deviations for n=3 independent experiments. **d,**
206 Experimental design for acetate labelling in co-culture. Briefly, AML cells are co-cultured with
207 stromal cells for 24 hours prior to addition of [2-^{13}C]acetate (extra 4 mM). After 8 hours of the
208 addition of acetate, cells are separated, and metabolites are extracted. **e,** ^{13}C percentages on polar
209 metabolites in SKM-1 and MS-5 cells in co-culture. Cells were co-cultured for 24 hours before the
210 addition of extra 4 mM sodium [2-^{13}C]acetate. Bars represent the mean of the ^{13}C percentage and
211 error bars represent the standard deviations of n=3 independent experiments. For C and E, ^{13}C
212 natural abundance is represented as a black bar at %^{13}C = 1.1.

213

214 **Transcriptomic data highlights a metabolic rewiring of stromal cells in co-culture characterised by**
215 **upregulation of glycolysis and downregulation of pyruvate dehydrogenase**

216 After establishing that stromal cells are responsible for acetate secretion (Fig. 1d) and that AML cells
217 consumed the secreted acetate in co-culture (Fig. 2d), we sought to elucidate the mechanism behind
218 acetate secretion by MS-5 cells in co-culture. Thus, we set out to perform global gene expression
219 profiling by RNA-seq comparing cells cultured alone and in co-culture (Supplementary Fig. 4a). With
220 this approach we identified 587 differentially expressed genes (q-value<0.1) (Supplementary Fig. 4b);
221 with 476 genes being upregulated and 111 genes being downregulated in co-culture.

222 Following clustering of differentially expressed genes, gene set enrichment analysis (GSEA) was
223 performed (Fig. 3a) revealing a positive correlation with the expression of genes that are part of the
224 glycolysis pathway (MSigDB: M5937) as well as the reactive oxygen species pathway (MsigDB:
225 M5938) (Fig. 3b).

226 A closer examination of the genes involved in the glycolysis pathway revealed a major upregulation
227 of several glycolysis-related genes in MS-5 cells in co-culture (Fig. 3c). Most of the genes involved in
228 glucose transport (*Slc2a1* and *Slc2a4*) and glucose breakdown to pyruvate (*Pgm1*, *Hk2*, *Gpi1*, *Pfkl*,
229 *Gapdh*, *Pgk1*, *Pgam1-2*, *Eno1-1b-2* and *Pkm*) were upregulated, including the gene encoding for the
230 6-phosphofructo-2-kinase/fructose-2,6-biphosphatase 3 (*Pfkfb3*), a well-known activator of
231 glycolysis.

232 In contrast, individual examination of genes related to pyruvate metabolism revealed that the genes
233 related to pyruvate conversion to acetyl-CoA were downregulated (Fig. 3c). Pyruvate transport into
234 the mitochondria (*Mpc1-2*) and several pyruvate dehydrogenase (PDH) complex-related genes
235 (*Pdha1*, *Pdhb* and *Pdhx*), involved in the conversion of pyruvate to acetyl-CoA, remained largely
236 unaltered or were slightly downregulated by co-culture. Additionally, the pyruvate dehydrogenase
237 kinases (*Pdk1*, *Pdk2* and *Pdk4*), which inhibit the activity of the PDH complex, were found to be
238 upregulated by co-culture. Interestingly, the acetyl-CoA synthetases (ACSs), which can generate
239 acetyl-CoA from acetate but have also been reported to perform the reverse reaction, encoded by
240 *Acss2* and *Acss3*, were found to be slightly upregulated in co-culture. Pyruvate can also be converted
241 to 2-oxaloacetate via pyruvate carboxylase (*Pcx*), to lactate by lactate dehydrogenase (*Ldha*), and to
242 alanine via alanine transaminase (*Gpt*). Only *Ldha* was found to be moderately upregulated in co-
243 culture. However, we did not observe a substantial increase in lactate production experimentally in
244 co-culture. Altogether, transcriptomic data suggests that MS-5 cells in co-culture present a major
245 upregulation of glycolysis and downregulation of the PDH complex.

246 To explore whether glycolysis is upregulated at a metabolic level in MS-5 cells in co-culture at the
247 metabolic level and whether acetate could derive from glucose, we performed [U-^{13}C]glucose tracing
248 on AML and MS-5 cells cultured alone and in co-culture and analysed the label incorporation in
249 glycolysis-related extracellular metabolites (Fig. 3d). For the three AML cell lines tested, extracellular
250 acetate presented significantly higher label incorporations from [U-^{13}C]glucose in co-culture
251 compared to cell types cultured alone, providing evidence that the secreted acetate in co-culture
252 derives from glucose. Lactate and alanine, which can be synthesised from pyruvate, did not show
253 significant increases in label incorporation from [U-^{13}C]glucose in co-culture compared to each cell
254 type cultured alone for all the AML cell lines, with the exception of alanine in HL-60. Overall, these
255 results are in agreement with the transcriptomic data (Fig. 3c), highlighting that glucose metabolism
256 is upregulated in co-culture but also confirming that acetate derives from glycolysis.

257

3

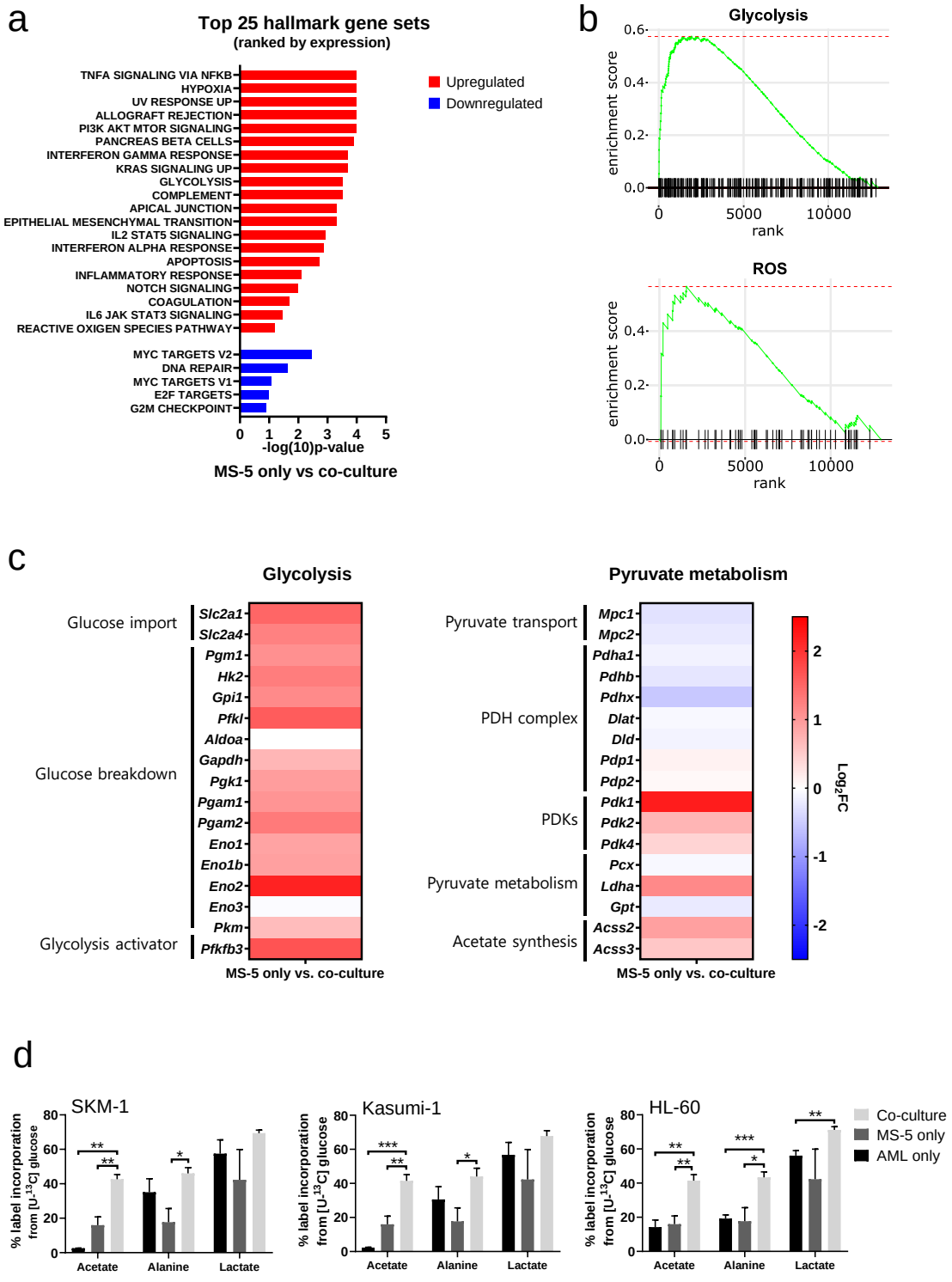
a
Top 25 hallmark gene sets
(ranked by expression)
TNFA SIGNALING VIA NFKB
HYPOXIA
UV RESPONSE UP
ALLOGRAFT REJECTION
PI3K AKT MTOR SIGNALING
PANCREAS BETA CELLS
INTERFERON GAMMA RESPONSE
KRAS SIGNALING UP
GLYCOLYSIS
COMPLEMENT
APICAL JUNCTION
EPITHELIAL MESENCHYMAL TRANSITION
IL2 STAT5 SIGNALING
INTERFERON ALPHA RESPONSE
APOPTOSIS
INFLAMMATORY RESPONSE
NOTCH SIGNALING
COAGULATION
IL6 JAK STAT3 SIGNALING
REACTIVE OXIGEN SPECIES PATHWAY
MYC TARGETS V2
DNA REPAIR
MYC TARGETS V1
E2F TARGETS
G2M CHECKPOINT
Upregulated
Downregulated
-log(10)p-value
MS-5 only vs co-culture
b
Glycolysis
enrichment score
rank
ROS
enrichment score
rank
c
Glycolysis
Glucose import
Slc2a1
Slc2a4
Glucose breakdown
Pgm1
Hk2
Gpi1
Pfkl
Aldoa
Gapdh
Pgk1
Pgam1
Pgam2
Eno1
Eno1b
Eno2
Eno3
Pkm
Glycolysis activator
Pfkfb3
MS-5 only vs. co-culture
Pyruvate metabolism
Pyruvate transport
Mpc1
Mpc2
PDH complex
Pdha1
Pdhb
Pdhx
Dlat
Dld
Pdp1
Pdp2
PDKs
Pdk1
Pdk2
Pdk4
Pyruvate metabolism
Pcx
Ldha
Gpt
Acetate synthesis
Acss2
Acss3
MS-5 only vs. co-culture
Log2FC
d
SKM-1
Kasumi-1
HL-60
% label incorporation from [U-13C] glucose
Acetate
Alanine
Lactate
Co-culture
MS-5 only
AML only

258
259

260 **Fig. 3. Transcriptomic data reveals that stromal cell metabolism is shifted towards higher**
261 **glycolysis and ROS upon co-culture with AML cells. a,** Top 25 GSEA hallmark gene sets ranked
262 by expression in MS-5 cells only vs co-culture with SKM-1 cells, analysed using the collection of
263 hallmark gene sets from Molecular Signature Database with a false discovery rate threshold at 5%. P-
264 values for each pathway are presented as –log(10)p-value. **b,** GSEA enrichment score plots of
265 glycolysis and ROS generated using Sleuth 0.30.0 R statistical package. **c,** Fold change values of
266 detected gene transcripts (TPMs) related to glycolysis and pyruvate metabolism. FC values are
267 represented as log_2FC, red values indicate upregulation and blue values indicate downregulation in
268 MS-5 cells in co-culture. **d,** Label incorporation from [U-^{13}C]glucose into extracellular metabolites in
269 AML and MS-5 cells cultured alone or in co-culture after 24 hours. Bars represent the mean of n=3
270 independent experiments and error bars represent standard deviations.

271

272 **AML cells rewire stromal cell metabolism transferring ROS via gap junctions to obtain acetate**

273 Tracer-based data on MS-5 cells in co-culture revealed that acetate secreted in co-culture derives
274 from glucose (Fig. 3d). However, transcriptomic data on MS-5 cells in co-culture suggested that
275 acetate did not derive from pyruvate via acetyl-CoA (Fig. 3c). Moreover, acetate secretion was also
276 observed in MS5 cells grown in thiamine-free media (Supplementary Fig. 5a), confirming that the
277 acetate secretion was not dependent on keto acid dehydrogenases [28] and indicating that a different
278 mechanism must be responsible. An alternative mechanism of acetate synthesis involving a non-
279 enzymatic oxidative decarboxylation of pyruvate into acetate had previously been described [28-30].
280 This mechanism was reported to be mediated by ROS in mammalian cells and was linked to cells
281 prone to overflow metabolism under the influence of high rates of glycolysis and excess pyruvate.
282 Hence, we decided to investigate whether ROS might play a role in acetate secretion in our co-
283 culture system.

284 We first modulated ROS levels in AML cells and MS-5 cells cultured alone and in co-culture and
285 measured acetate production. Hydrogen peroxide was used to increase ROS levels and N-
286 acetylcysteine (NAC) was used as a ROS scavenger. Extracellular acetate levels were measured by ^{1}H-
287 NMR after 24 hours. Increasing ROS levels with peroxide resulted in a significant increase in acetate
288 secretion, particularly in SKM-1 and Kasumi cells in co-culture (Fig. 4a, Supplementary Fig. 5b)). This
289 experiment could not be carried out with HL-60 cells as peroxide treatment severely impaired the
290 viability of HL-60 cells, as previously reported [31]. Additionally, when the ROS scavenger NAC was
291 used, a significant decrease in the levels of acetate in both MS-5 cells cultured alone and in all the
292 co-cultured cell lines was observed (Fig. 4a, Supplementary Fig. 5b). Interestingly, the production of
293 acetate in cells in co-culture treated with NAC recovered the phenotype of MS-5 cells cultured alone,
294 indicating that acetate synthesis in MS-5 cells in co-culture is mediated by ROS (Fig. 4a).

295 Next, we compared intracellular ROS levels in AML and stromal cells in co-culture and cultured alone
296 by labelling cells with the H_2DCFDA fluorescent dye. Fluorescence measurements showed that ROS
297 levels in the three AML cell lines used were significantly decreased in co-culture, whilst in the
298 stromal cells ROS levels were significantly increased in two of the three co-cultures (Fig. 4b). These
299 results suggested that AML cells might transfer ROS to stromal cells. We also performed the same
300 experiment using three primary AML samples to corroborate the previous result. Fluorescence
301 analysis showed decreased ROS levels in AML samples in co-culture and increased ROS levels in MS-5
302 cells in co-culture for the three primary AML samples analysed (Fig. 4c), suggesting ROS transfer
303 from AML cells to stromal cells in co-culture.

304 To further test whether AML cells might transfer ROS through a contact-dependent mechanism, we
305 compared the intracellular ROS levels in AML and stromal cells cultured alone and co-cultured
306 without direct contact using a permeable membrane. Fluorescence measurements in both cell types
307 revealed that ROS levels remained unaltered in contact-free co-cultures (Fig. 4d), indicating that ROS
308 transfer could only occur via a contact-dependent mechanism.

309 As it had been previously reported that haematopoietic stem cells can transfer ROS to stromal cells
310 via gap junction to prevent senescence [32], we decided to examine gap junction genes in the
311 transcriptome of MS-5 cultured alone and in co-culture. When individually examining the gap
312 junction genes in MS-5 cells cultured alone vs co-culture, we found several gap junction genes
313 upregulated in co-culture such as *Gja5, Gja8, Gjb5* and *Gjc2* (Fig. 4e). These results suggest that AML
314 cells might establish gap junction interactions to transfer ROS to MS-5 cells when in co-culture. To
315 test this hypothesis, we used the calcein-AM dye, which can only be transferred via gap junctions [10].
316 We labelled stromal cells with calcein-AM, cultured them with unlabelled AML cells and analysed the
317 fluorescence of AML cells after three hours. We found that, for the three AML cell lines tested, the
318 percentage of cells that had incorporated the calcein-AM dye from MS-5 cells was larger than 80%
319 (Fig. 4f, Supplementary Fig. 5c), indicating that AML cells can establish gap junctions with stromal
320 cells when co-cultured in direct contact.

321 Next, we decided to confirm that AML cells can transfer ROS via gap junctions by inhibiting the gap
322 junctions using carbenoxolone (CBX), a well-known gap junction inhibitor [10,33,34]. We first confirmed
323 that efficiency of inhibition by analysing the calcein-AM dye transfer in a control and treated co-
324 culture of SKM-1 and MS-5 cells. The CBX treatment reduced the calcein-AM transfer more than 60%
325 in co-culture (Fig. 4g). We then compared intracellular ROS levels in both AML and stromal cells
326 treated with CBX and control. CBX treatment abrogated the decrease in ROS levels in AML cells (Fig.
327 4h) and the increase of ROS levels in stromal cells (Fig. 4i), indicating inhibition of ROS transfer in
328 CBX treated co-cultures. Overall, this result provides strong evidence that ROS transfer occurs via
329 gap junctions established between AML and stromal cells.

330

4

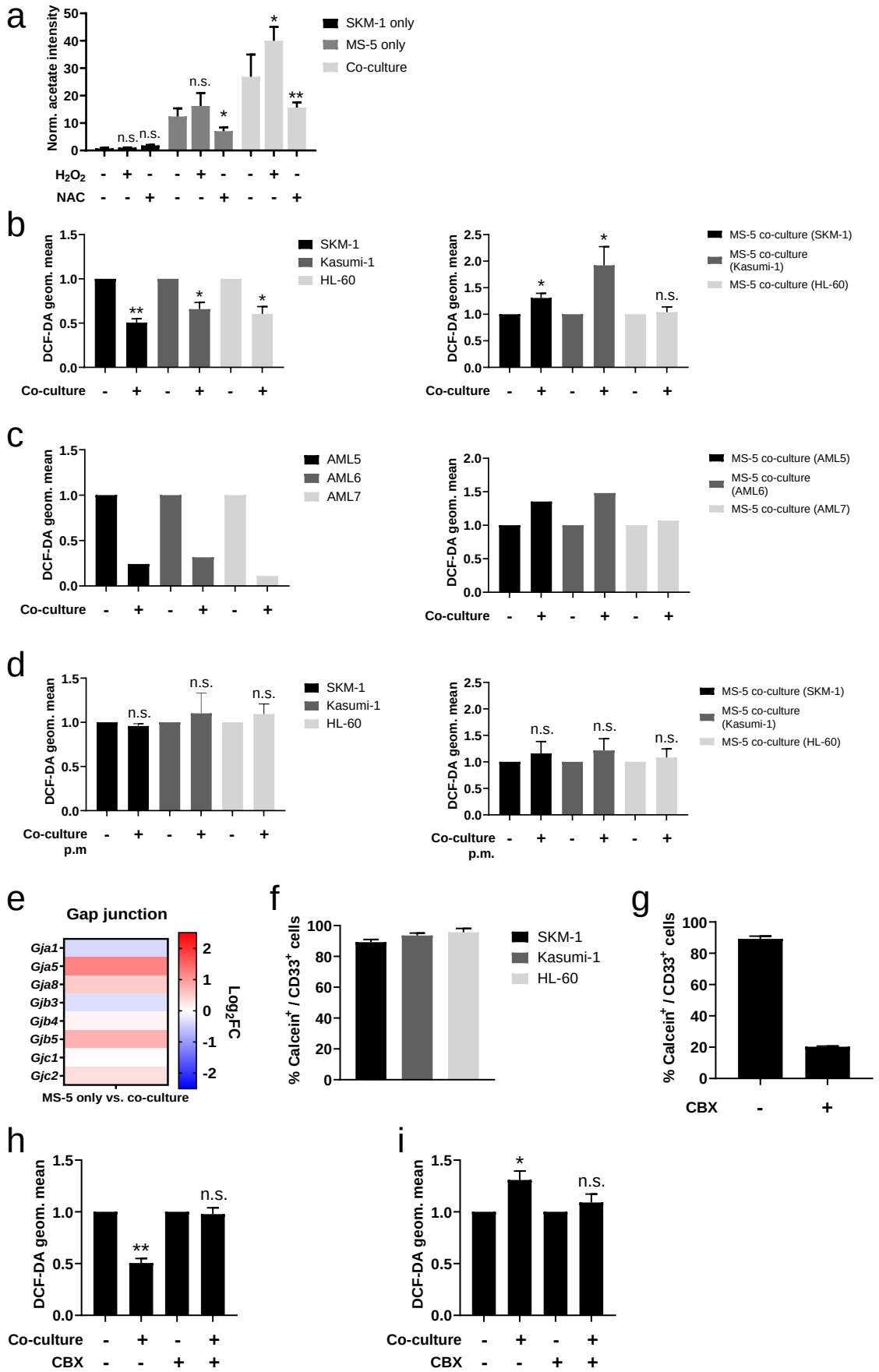
a
Norm. acetate intensity
SKM-1 only
MS-5 only
Co-culture
n.s.
n.s.
n.s.
*
*
**
H2O2 - + - - + - - + -
NAC - - + - - + - - +
b
DCF-DA geom. mean
SKM-1
Kasumi-1
HL-60
Co-culture - + - + - +
MS-5 co-culture (SKM-1)
MS-5 co-culture (Kasumi-1)
MS-5 co-culture (HL-60)
c
AML5
AML6
AML7
MS-5 co-culture (AML5)
MS-5 co-culture (AML6)
MS-5 co-culture (AML7)
d
Co-culture p.m
Co-culture p.m.
e
Gap junction
Gja1
Gja5
Gja8
Gjb3
Gjb4
Gjb5
Gjc1
Gjc2
MS-5 only vs. co-culture
Log2FC
f
% Calcein+ / CD33+ cells
g
CBX - +
h
CBX - - + +
i

331

332 **Fig. 4. Acetate secretion is linked to ROS transfer from AML to stromal cells via gap**
333 **junctions. a,** Extracellular acetate levels in SKM-1 (black) and MS-5 cells cultured alone (dark grey)
334 and in co-culture (light grey) for 24 hours in a control medium, medium with 50 µM H_2O_2 or medium
335 with 5 mM NAC. **b**, **c** and **d** Intracellular ROS levels measured by H_2DCFDA staining in **b** and **d** AML
336 cells or **c** primary patient-derived AML cells and MS-5 cells cultured alone and in co-culture in **b** and **c**
337 direct contact or **e,** fold change values of detected gene transcripts (TPMs) related to gap junctions.
338 FC values are represented as log_2FC, red values indicate upregulation and blue values indicate
339 downregulation in MS-5 cells in co-culture. **f,** Frequencies of Calcein-AM and CD33 positive AML cell
340 lines after being in co-culture with Calcein-AM stained MS-5 cells for 3 hours. **g,** Frequencies of
341 Calcein-AM and CD33 positive SKM-1 cells (treated or untreated with 200 µM carbenoxolone for 24
342 hours) after being in co-culture with Calcein-AM stained MS-5 cells for 3 hours. **h** and **i** Intracellular
343 ROS levels measured by H_2DCFDA staining in **h** AML cells and **i** MS-5 cells cultured alone and in co-
344 culture in direct contact treated or untreated with 200 µM carbenoxolone for 24 hours. **j,** Cell
345 viability was assessed in SKM-1 cells cultured with 5-azacytidine or DMSO, with and without NAC
346 over 48 hours by trypan blue staining and counting. Each point represents the mean and error bars
347 represent the standard deviations of n=3 independent experiments. For **a**, **b**, **c**, **d**, **f**, **g**, **h** and **i** bars
348 represent the mean of n=3 independent experiments and error bars represent standard deviations.
349 For **a**, **b**, **d**, **h** and **i** and **j** unpaired Student's t-test was applied for **a** each condition (H_2O_2/NAC) was
350 compared to untreated; for **b**, **d**, **h** and **i** co-culture conditions were compared to cells cultured
351 alone; for **j** each pair of conditions was compared (black brackets). P-values are represented by n.s.
352 for not significant, * for p-value<0.05, ** for p-value<0.01 and *** for p-value<0.001.

353

354 **Discussion**

355 AML cells are known to interact and remodel niche cells through various mechanisms, including the
356 secretion of soluble factors, cytokines or metabolites, resulting in a better support of AML cells at
357 the expense of normal haematopoiesis. Yet, metabolic crosstalk between AML and stromal cells has
358 not been reported before. Here, we have identified a novel metabolic communication between AML
359 and stromal cells mediated by acetate. Our in vivo data shows high acetate levels in the bone
360 marrow extracellular fluid of AML but not in healthy control mice, indicative of a potential role for
361 acetate in AML development. Our in vitro data suggests that AML cells can modulate stromal cells
362 into secreting acetate in co-culture, by rewiring stromal cell metabolism, and can then utilise the
363 secreted acetate to feed their own TCA cycle to generate energy. Mechanistically, our data revealed
364 that acetate secretion involves not only a higher glycolytic rate but also the non-enzymatic ROS-
365 mediated conversion of pyruvate to acetate, as cells grown in thiamine-free media were still capable
366 to produce acetate. Furthermore, our data indicates that AML cells can diminish their ROS levels by
367 establishing gap junctions with stromal cells facilitating ROS transfer to stromal cells.

368 Studying the interactions between cancer cells and their microenvironment in terms of metabolism
369 has become an exciting new field of cancer research. Our data indicates that AML cells can influence
370 the metabolism of stromal cells causing increased acetate secretion, which was not observed in
371 healthy counterparts. We presented several lines of evidence suggesting that stromal cells but not
372 AML cells are responsible for acetate secretion: (i) stromal cells cultured alone secreted acetate,
373 whilst AML cell lines and primary AML cells did not; (ii) after separating stromal cells from co-culture
374 with AML cell lines, stromal cells continued to secrete acetate at a similar rate to that observed in
375 co-culture; and, (iii) glycolysis was upregulated in stromal cells in co-culture, and glucose was found
376 to be the precursor of the secreted acetate in co-culture.

377 Interestingly, acetate has been reported as an alternative fuel for cancer cells [35,36], especially under
378 low oxygen conditions or lipid depletion [37-39], but it has not previously been described to participate
379 in crosstalk between any type of cancer cells and their microenvironment. Nonetheless, other
380 monocarboxylate metabolites, such as lactate and alanine, have been reported to participate in
381 different types of metabolic interplay between stromal and cancer cells [40-42]. Our work reveals that
382 aside from lactate and alanine, other monocarboxylate metabolites, such as acetate, can be utilised
383 by leukaemic cells as a biofuel. Although acetate usage to feed the TCA cycle had already been
384 described in AML [43] and other types of cancer [38,44], this is, to our knowledge, the first report of AML
385 cells utilising acetate secreted by stromal cells in co-culture.

386 We have also proposed a mechanism for the altered stromal cellular metabolism, involving
387 increased glycolysis and the ROS-mediated chemical conversion of pyruvate to acetate.
388 Transcriptomics showed that glycolysis is upregulated in stromal cells in co-culture, and tracer-based
389 metabolism using [U-^{13}C]glucose, demonstrated that more label gets incorporated in pyruvate and
390 acetate in stromal cells in co-culture compared to either AML or stromal cells cultured alone.
391 Enrichment of hypoxia genes and elevated Pdk expression have been reported to be related to
392 higher glycolytic activity [45-47]. Similarly, other cancer cells [48-51] have also been shown to modulate
393 stromal metabolism by increasing glycolysis. Moreover, this mechanism was further supported by
394 increasing and lowering ROS levels in co-culture. Lowering ROS levels recovered the acetate
395 secretion phenotype of MS-5 cells cultured alone.

396 AML cells are known to exhibit high levels of ROS [52,53]. However, our data has shown that AML cells
397 in co-culture present lower levels of ROS than AML cells cultured alone, which is in agreement with
398 recent studies in primary AML and mesenchymal stromal cell co-cultures [14,24]. The current
399 mechanisms to describe this phenomenon involve mitochondrial transfer and activation of
400 glutathione-related antioxidant pathways [14,24], although previous data on haematopoietic stem cells
401 (HSCs) revealed that HSCs can directly transfer ROS via gap junctions to stromal cells [32]. Interestingly,
402 our data showed that the decrease in ROS levels was counteracted by inhibiting contact using a
403 permeable membrane. We also found several gap junction genes upregulated in stromal cell types in
404 co-culture. Moreover, we prevented ROS transfer from AML to stromal cells by using the gap
405 junction inhibitor CBX [10,33,34]. Thus, our results suggest that ROS transfer via gap junctions, at least
406 partially, mediates the mechanism behind AML cells presenting lower levels of ROS in co-culture.

407 Overall, this work reveals a unique and novel metabolic communication between AML and stromal
408 cells that involves acetate as the main crosstalk metabolite. We showed that AML cells are capable
409 of modulating the metabolism of stromal cells by transferring ROS via gap junctions resulting in an
410 increased secretion of acetate and its subsequent accumulation in the extracellular medium, which
411 correlates with the observation of higher acetate levels in the bone marrow extracellular fluid of
412 AML mice compared to control mice. Furthermore, we found that AML cells consume the secreted
413 acetate and use it as an energy source, by fluxing it into the TCA cycle. We believe our findings
414 provide a better understanding of how AML cells communicate with stromal cells and could serve as
415 a basis for the development of novel therapeutic strategies to target AML cells by modulating gap
416 junction formation as an adjuvant therapy.

417

418 ## Materials and Methods

419 ### Cell lines

420 The human AML cell lines (SKM-1, Kasumi-1 and HL-60), the mouse stromal cell line (MS-5) and the
421 human cervical cancer cell line (HeLa) were cultured in RPMI 1640 media supplemented with 15%
422 (v/v) FBS, 2 mmol/L L-glutamine and 100 U/ml Penicillin/Streptomycin (all from Thermo Fisher
423 Scientific). Co-cultures were plated in a 4:1 AML-stromal ratio, and 750.000 cells/ml density of AML
424 cells over confluent stromal cells. Prior to cell extraction for NMR, RNA collection or protein
425 extraction, a suspension of 10 million AML cells was collected, the stromal layer was washed with
426 PBS and was subject to mild trypsinisation with 1:5 dilution of 0.25% Trypsin 1 mM EDTA
427 (Thermofisher) to remove attached residual leukaemic cells before completely detaching stromal
428 cells with 0.25% Trypsin-EDTA.

429 ### Primary patient samples

430 AML and PBMC primary specimens' procedures were obtained in accordance with the Declaration of
431 Helsinki at the University Medical Center Groningen, approved by the UMCG Medical Ethical
432 Committee or at the University Hospital Birmingham NHS Foundation Trust, approved by the West
433 Midlands – Solihull Research Ethics Committee (10/H1206//58).

434 Additional information about the primary AML samples used in this study can be found in Annex 1.
435 Peripheral blood (PB) and bone marrow samples from AML patients and healthy donors were
436 obtained in heparin-coated vacutainers. Mononuclear cells were isolated using Ficoll-Paque (GE
437 Healthcare) and stored at -80°C.

438 For AML1-2 and PBMC1-2, samples were thawed and resuspended in newborn calf serum (NCS)
439 supplemented with DNase I (20 Units/mL), 4 mM $MgSO_4$ and heparin (5 Units/mL) and incubated on
440 37°C for 15 minutes (min). For AML1 and PBMC1, cells were sorted after thawing by fluorescence-
441 activated cell sorting (FACS) for the CD34+CD38- population using 10 µL of anti-CD34 APC (560940,
442 BD Biosciences), 10 µL of anti-CD38 FITC (555459, BD Biosciences) and 10 µL of DAPI (D1306, Thermo
443 Fisher Scientific) per 10 million cells. Cells were sorted using a Sony SH800S (Sony) sorter. For AML2
444 and PBMC2, cells were thawed and the CD34+ population was sorted by magnetic-activated cell
445 sorting (MACS) using 10 µL of anti-CD34 microbeads (130-046-702, Miltenyi) per million of expected
446 CD34 cells following manufacturer's protocol.

447 AML1-2, PBMC1-2 and MS-5 cells were cultured alone and in co-culture in a 4:1 AML/PBMC-stromal
448 ratio and 500,000 cells/mL density in α-MEM (Gibco) with 12.5% (v/v) FCS (Sigma-Aldrich), 1% (v/v)

449 Pen/Strep (Thermo Fisher Scientific), 12.5% (v/v) Horse serum (Invitrogen), 0.4% (v/v) β-
450 mercaptoethanol (Merck Sharp & Dohme BV) and 0.1% hydrocortisone (H0888, Sigma-Aldrich). For
451 AML1 and AML2 the medium was supplemented with 0.02 µg/mL of IL-3 (Sandoz), 0.02 µg/mL
452 NPlate (Amgen) and 0.02 µg/mL of G-CSF (Amgen). For PBMC1 and PBMC2 the medium was
453 supplemented with 100 ng/ml of human SCF (255-SC, Novus Biologicals), 100 ng/ml of NPlate, 100
454 ng/ml of FLT3 ligand (Amgen) and 20 ng/ml of IL-3. Samples of medium were collected at 0 and 48
455 hours.

456 AML3 - 7 and PBMC3 were thawed and kept in culture for 16-24 hours in Stem Span H3000 media
457 (STEMCELL Technologies) supplemented with 50 µg/ml ascorbic acid (Sigma-Aldrich), 50 ng/ml
458 human SCF (255-SC-010, R&D Systems), 10 ng/ml human IL-3 (203-IL-010, R&D Systems), 2 units/ml
459 human-erythropoietin (100-64, PeproTech), 40 ng/ml insulin-like growth factor 1 (IGF-1) (100-12,
460 PeproTech), 1 µM dexamethasone (D2915, Sigma-Aldrich) and 100 µg/ml primocin (ant-pm-2,
461 InvivogenCD34+ cKit+ cells were purified using magnetic microbeads (130-046-702 (CD34) and 130-
462 091-332 (CD117), Miltenyi Biotec). Cells were cultured in the supplemented Stem Span media for 24
463 hours prior to co-culture setting. Co-cultures were plated with a 4:1 leukaemic to stromal cells ratio
464 and a 300,000 cells/ml density in supplemented Stem Span medium. Samples of leukaemic/healthy
465 cells and MS-5 cells alone were also cultured in supplemented Stem Span media as controls. Samples
466 of medium were collected at 0 and 48 hours.

467 **In vivo experiments**

468 12 weeks old C57BL6/J female mice (The Jackson Laboratory) were lethally irradiated with 9Gy (2
469 doses of 4.5Gy separated by 3h) using an X-RAY source (Rad Source's RS 2000). Mice were
470 transplanted by intravenous injection 4h after with $2x10^6$ bone marrow (BM) nucleated cells isolated
471 as previously described [54] from leukemic male mice heterozygous for MLL-AF9 knock-in fusion
472 transgene or wild-type (WT) control male littermates [55] . Male transgenic and WT control MLL-AF9
473 were purchased from The Jackson Laboratory (Stock No: 009079) and were 6 months old when
474 euthanized to allow development of signs of leukemic transformation driven by the MLL-AF9 fusion
475 oncogene in transgenic animals. MLL-AF9 expression in BM cells derived from transgenic donors
476 results in development of AML with high blast counts in recipients. Recipients were euthanized 6
477 months after the transplant, bone marrow from femur and tibia was flushed with a syringe in 150 µL
478 of cold PBS and centrifuged at 15000g for 10 minutes at 4^oC. The supernatant made of bone marrow
479 extracellular fluid (BMEF) was kept for analysis of acetate level. Experiments were conducted with
480 the ethical approval of the Norwegian Food and Safety Authority. Animals were housed under

481 specific opportunistic and pathogen free environment at the Animal Facility of the University of Oslo,
482 Norway.

483

484 **Proliferation analysis using CFSE**

485 The CellTrace™ carboxyfluorescein succinimidyl ester (CFSE) Cell Proliferation Kit (C34570,
486 Invitrogen) was used to assess proliferation of AML cells following the manufacturer's protocol. AML
487 cells were stained and their fluorescence was assessed before dividing the bulk of cells into culturing
488 them alone or with MS-5 cells for 48 hours. Small aliquots of cells after 24 and 48 hours were
489 analysed by flow cytometry. Flow cytometry analysis was carried out in a CyAn ADP flow cytometer
490 (Beckman Coulter). Data analysis was performed using the FlowJo software package (BD).

491 **Carbenoxolone treatment**

492 Carbenoxolone (CBX) disodium salt (Sigma-Aldrich, C4790) was prepared fresh at 200 µM in cell
493 culture medium. Cells were resuspended in the CBX medium and cultured alone or in co-culture for
494 24 hours prior to ROS or Calcein-AM dye transfer experiments.

495 **Cellular ROS measurements using DCFH-DA**

496 Cellular ROS was measured by incubating cells with 100 µM 2',7'-Dichlorofluorescin diacetate (DCFH-
497 DA) (D6883, Sigma-Aldrich) in Hank's Balanced Salt Solution (HBSS) (Thermo Fisher Scientific) at 37°C
498 for 30 min protected from light. Cells were then harvested and stained with 5 µg/µL anti-human
499 CD33 eFluor 450 (eBioscience, P67.6) for 30 min at 4°C before flow cytometry analysis as previously
500 described.

501 **Thiamine-free medium comparison**

502 Thiamine-free medium (R9011-01, United States Biological) was prepared as per manufacturer
503 instructions and supplemented with 10% dialised FBS.

504 MS-5 cells were cultured in thiamine-free medium or control RPMI medium for 4 days prior to the
505 experiment. Cells were then seeded with fresh thiamine-free or control RPMI medium and incubated
506 for 24 hours. Samples of medium were collected at 0 and 24 hours and kept at -80ºC.

507 **ROS-related treatments with H_2O_2 and NAC**

508 SKM-1, Kasumi, HL-60 and MS-5 cells cultured alone and in co-culture were incubated for 24 hours in
509 50 µM H_2O_2 (Merck) complete cell culture medium, 5 mM N-acetylcysteine (NAC) (106425, Merck)

510 complete cell culture medium or control medium. Samples of medium were collected at 0 and 24
511 hours and kept at -80°C.

512

513 **Calcein-AM dye transfer assay**

514 Functional gap junction presence was evaluated using the fluorescent dye Calcein-AM green
515 (Invitrogen, C1430) adapting a previously established protocol [10]. MS-5 cells were stained with 500
516 nM Calcein-AM dye in complete cell culture medium for 1 hour at 37°C. Stained cells were washed
517 with serum-free medium for 30 min at 37°C before being co-cultured with AML cells for 3h. AML
518 cells were then harvested and stained with 5 µg/µL anti-human CD33 eFluor 450 (eBioscience,
519 P67.6) for 30 min at 4°C before flow cytometry analysis as previously described. Calcein-AM dye
520 transfer was quantified as the frequency of $CD33^+$ and Calcein-AM^+ cells.

521 **Tracer-based NMR experiments**

522 [U-^{13}C]Glucose (CC860P1, CortecNet) was added to RPMI 1640 medium without glucose (11879020,
523 Merck) to a final concentration of 2 g/L (as in the complete cell culture medium) and was
524 supplemented as usual with 15% (v/v) FBS, 2 mmol/L L-glutamine and 100 U/mL Pen/Strep. The
525 medium was prepared fresh and was filtered with a 0.2 µm syringe filter (Sartorius) before each
526 experiment.

527 4 mM sodium [2-^{13}C]acetate (279315-1G, Sigma-Aldrich) was added to complete cell culture medium
528 and the medium was filtered with a 0.2 µm syringe filter before each experiment. Cells were
529 incubated for the time indicated in each experiment before separation of cells and/or metabolite
530 extraction. **a**, **b**, **c**, **d**, **f**, **g**, **h** and **i** Unlabelled samples were prepared as a control for 2D-NMR
531 experiments and to measure acetate consumption by adding unlabelled sodium acetate trihydrate
532 (1.37012, Merck) to complete cell culture medium before metabolite extraction or collection of
533 medium samples.

534 **Metabolite extraction**

535 Suspension cells and detached adherent cells were washed with PBS before being rapidly
536 resuspended in 400 µl of HPLC grade methanol pre-chilled on dry ice. Samples were transferred to
537 glass vials and were subject to 10:8:10 methanol-water-chloroform extraction as described in
538 (Saborano 2019). Polar phase samples were evaporated in a SpeedVac concentrator and were
539 subsequently kept at -80°C.

540 **Sample preparation for NMR**

541 Medium samples or bone marrow extracellular fluid samples were mixed with a D_2O phosphate
542 buffer containing TMSP ((3-trimethylsilyl)propionic-(2,2,3,3-d_4)-acid sodium salt) and NaN_3 to a final
543 concentration of 0.1 M phosphate and 0.5 mM TMSP ((3-trimethylsilyl)propionic-(2,2,3,3-d_4)-acid
544 sodium salt) and 1.5 mM NaN_3 (all from Sigma) and transferred to 3 mm NMR tubes (Cortecnet).

545 Dried polar extracts for tracer-based NMR experiments were reconstituted in 50 µL of 0.1 M
546 phosphate buffer in 100% D_2O with 3 mM NaN_3 and 0.5 mM TMSP. Samples were sonicated for 10
547 min and transferred to 1.7 mm NMR tubes using a micro pipet system. Samples were prepared
548 freshly before the acquisition.

549 **NMR acquisition and analysis**

550 All NMR data were acquired on Bruker 600MHz spectrometers equipped with Avance-III consoles
551 using cooled Bruker SampleJet autosamplers. For media samples, a 5mm triple resonance cryoprobe
552 (TCI) z-axis pulsed field gradient (PFG) cryogenic probe was used, and for cell extracts, a TCI 1.7mm
553 z-PFG cryogenic probe was used. Probes were equipped with a cooled SampleJet autosampler
554 (Bruker) and automated tuning and matching.

555 For medium samples, spectra were acquired at 300K using 1D ^{1}H-NOESY (Nuclear Overhauser effect
556 spectroscopy) pulse sequence with pre-saturation water suppression (noesygppr1d, standard pulse
557 sequence from Bruker). The spectral width was 12 ppm, the number of data points was TD 32,768,
558 the interscan delay was 4 sec and the NOE mixing time was 10 msec. The ^{1}H carrier was set on the
559 water frequency and the ^{1}H 90º pulse was calibrated at a power of 0.256 W and had a typical length
560 of ca 7-8 µs. 64 scans and 8 dummy scans were acquired and the total experimental time was 7.5
561 min. Spectra were processed using the MetaboLab [56] software within the MATLAB environment
562 (MathWorks). A 0.3Hz exponential apodization function was applied to FIDs followed by zero-filling
563 to 131,072 data points prior to Fourier transformation. The chemical shift was calibrated by
564 referencing the TMSP signal to 0 ppm and spectra were manually phase corrected. The baseline was
565 corrected by applying a spline baseline correction, the water and edge regions of the spectra were
566 excluded before scaling the spectra using a probabilistic quotient normalization (PQN). Chenomx 7.0
567 software (Chenomx Inc.) and the human metabolome database (HMDB) were used to assign the
568 metabolites present in the acquired spectra. Metabolite signal intensities were obtained directly
569 from the spectra and were normalised to a control medium sample obtained at time 0 hours. For
570 bone marrow extracellular fluid samples, metabolite signal areas were obtained directly from the
571 spectra.

572 For ^{13}C-filtered ^{1}H-NMR experiments, [U-^{13}C]glucose labelled medium samples were analysed with
573 ^{13}C-filtered ^{1}H-NMR spectroscopy as described in [57]. Spectra were acquired at 300 K using a double
574 gradient BIRD filter pulse sequence developed in-house [57]. A pulse program combining the ^{1}H[^{12}C]
575 and the all-^{1}H experiments in scan-interleaved mode was used. The difference between the two FIDs
576 gave the ^{1}H[^{13}C] signal. The spectral width was 12 ppm, the number of data points was 16,384 in
577 each dimension and the relaxation delay was 5.3 sec. 256 scans with 64 dummy scans were acquired
578 and the experimental time was 15 min. ^{13}C-filtered ^{1}H-NMR spectra were processed in Topspin 4.0.5
579 (Bruker). Spectra were zero filled to 32,768 data points before Fourier transformation. Phase
580 correction was applied to the ^{1}H[-^{12}C] and the all-^{1}H spectra and the difference ^{1}H[^{13}C] spectrum was
581 obtained by aligning on chemical shift. Metabolites were selected in the ^{1}H[^{13}C] spectrum and
582 integrated in all the spectra (^{1}H[^{12}C], ^{1}H[^{13}C] and all-^{1}H). Label incorporations (^{13}C percentages) were
583 calculated by dividing the signal areas obtained in the ^{1}H[^{13}C] spectrum by the ones obtained in the
584 all-^{1}H spectrum.

585 For ^{1}H-^{13}C-HSQC experiments, spectra were acquired using a modified version of Bruker's
586 hsqcgphprsp pulse program, with additional gradient pulses during the INEPT echo periods and using
587 soft 180º pulses for ^{13}C. For the ^{1}H dimension, the spectral width was 13.018 ppm with 2048
588 complex points. For the ^{13}C dimension, the spectral width was 160 ppm with 2048 complex points. 2
589 scans were acquired per spectrum and with an interscan delay of 1.5 sec. Non-uniform sampling
590 (NUS) with a 25% sampling schedule (generated using the Wagner's schedule generator (Gerhard
591 Wagner Lab, Harvard Medical School) with a tolerance of 0.01 and default values for the other
592 parameters) was used with 4096 increments yielding 8192 complex points after processing. The total
593 experimental time was 4 hours. Spectra were processed and phased with NMRPipe (National
594 Institute of Standards and Technology of the U.S.) (Appendix 8.1). MetaboLab was used to reference
595 the chemical shift using the signal for the methyl group of L-lactic acid, at 1.31/22.9 ppm in the ^{1}H
596 and ^{13}C dimensions, respectively. Identification of metabolites in 2D spectra was carried out using
597 the MetaboLab software which includes a chemical shift library for ca. 200 metabolites. Intensities
598 were obtained from signals in the spectra and were corrected for differences in cell numbers
599 contributing to the sample as follows: A ^{1}H-NMR spectrum was acquired for each sample and the
600 total metabolite area of this spectrum after removal of the water and TMSP reference signal was
601 calculated in MetaboLab. The intensities in the 2D spectra were then divided by the total metabolite
602 area of the corresponding ^{1}H-NMR spectrum. To obtain the % of ^{13}C in a metabolite, the normalized
603 intensity of a certain carbon in the labelled sample was divided by the normalized intensity of the
604 same carbon in the unlabelled sample and was multiplied by the natural abundance of ^{13}C (1.1%).

605 **RNA extraction and sequencing**

606 MS-5 cells were cultured alone or in co-culture with SKM-1 cells for 24 hours. Cells were separated
607 and washed with PBS prior to RNA extraction with TRIzol (Gibco) according to the manufacturer's
608 protocol. RNA was purified with RNeasy Plus Micro kit. Samples were sent to Theragenetex to be
609 sequenced with Novaseq 150bp PE with 40M reads.

610

611 **Real-time PCR**

612 Samples of RNA from SKM-1 and MS-5 co-cultures were collected and extracted using Trizol
613 (Invitrogen) following manufacturer's protocol. cDNA was synthesized using the M-MLV reverse
614 transcriptase (Promega) according to manufacturer's instructions. For gene expression analysis, qRT-
615 PCR of *Hk2* (NM_013820), *Pdhx* (NM_175094), *Pdk1* (NM_172665) and *Pdk2* (NM_133667) (all
616 KiCqStart™ primers KSPQ12012, Sigma Aldrich) were carried out using the SYBRGreen Master mix
617 (Thermo Fisher Scientific) and qRT-PCR of *B2m* (NM_009735.3, TaqMan® assays, Thermo Fisher
618 Scientific) was performed using TaqMan PCR Master Mix (Thermo Fisher Scientific). Reactions were
619 performed in a Stratagene Mx3000P and were run in triplicate. Relative gene expression was
620 calculated following the $2^{-\Delta\Delta Ct}$ method relative to the expression of *B2m*.

621 **RNA sequencing**

622 RNA samples of MS-5 cells cultured alone and in co-culture with SKM-1 cells extracted using Trizol
623 were purified using the Rneasy Plus Micro kit (Qiagen) according to manufacturer's protocol.
624 Transcriptome analysis was performed by Theragen Etex Co., LTD. (www.theragenetex.net). cDNA
625 libraries were prepared with the TruSeq Stranded mRNA Sample Prep Kit (Illumina) and RNA
626 sequencing was performed in a HiSeq2500 platform (Illumina). Quality control metrics were
627 obtained with FastQC 0.11.7 software (Babraham Bioinformatics). To quantify transcript abundances
628 using the Kallisto 0.43.0 software (Patcher Lab), read counts were aligned to the GRCm38 mouse
629 reference genome cDNA index (Ensembl rel.67). Gene-level differential expression analysis was
630 carried out with the R statistical package Sleuth 0.30.0 comparing the expression of cells cultured
631 alone vs co-culture. Differentially expressed genes were calculated using the Wald statistical test,
632 correcting for multiple testing with the Benjamin-Hochberg method. The false discovery rate (FDR)
633 threshold was set at 1% (q-values < 0.01). Ensembl gene transcripts were annotated to Entrez IDs
634 and official gene symbols with the R statistical package BioMart 2.40.3. To normalise for sequencing
635 depth and gene length, transcripts per million (TPM) expression values were calculated. Gene Set
636 Enrichment Analysis (GSEA) was performed with the R statistical package fgsea 1.10.0. The collection

637 of hallmark gene sets from the Molecular Signature Database was used for the GSEA, setting the FDR
638 threshold at 5%. Data was deposited in GEO (GSE163478).

639

640 **Acknowledgements**

641 N. Vilaplana-Lopera, G. Papatzikas, A. Cunningham, and A. Erdem were supported by the EU grant
642 HaemMetabolome H2020-MSCA-ITN-2015-675790. U. Günther, P. Garcia, J. J. Schuringa, J.-B. Cazier,
643 and F. Schnütgen acknowledge support from the European Commission (HaemMetabolome [EC-
644 675790]). This work was further supported by the Deutsche Forschungsgemeinschaft (DFG, German
645 Research foundation) SFB815, TP A10 (F.S.). We also acknowledge the Wellcome Trust for
646 supporting access to NMR instruments at the Henry Wellcome Building for Biomolecular NMR in
647 Birmingham (grant number 208400/Z/17/Z). The mouse work was supported by a joint meeting
648 grant of the Northern Norway Regional Health Authority and UiT (2014/5668) to L. Arranz. We thank
649 A. Villatoro and L.M. Gonzalez for technical assistance.

650 **Author Contributions**

651 N.V-L. conceived and performed the experiments, acquired, analysed and interpreted the data, and
652 wrote the manuscript. V.C., R.A., E.G., A.C., A.E., F.S., M.R., L.A. performed the experiments and
653 edited the manuscript. G.P. analysed the RNA-seq data. J.B helped with the experimental design. S.P.
654 and M.R. provided with patient samples. V.C. and L.A. provided mouse bone marrow extracellular
655 fluid samples. J.J.S. provided patient samples, helped with the experimental design, interpretation
656 and critical discussion of the data and edited the manuscript. U.G and P.G. conceived and performed
657 the experiments, acquired and interpreted the data, wrote the manuscript, and managed the
658 project.

659

660

661 **References**

662 1. Kreitz, J.*, et al.* Metabolic Plasticity of Acute Myeloid Leukemia. *Cells* **8**(2019).
663 2. Schelker, R.C.*, et al.* TGF-β1 and CXCL12 modulate proliferation and chemotherapy
664 sensitivity of acute myeloid leukemia cells co-cultured with multipotent mesenchymal
665 stromal cells. *Hematology* **23**, 337-345 (2018).
666 3. Passaro, D.*, et al.* Increased Vascular Permeability in the Bone Marrow Microenvironment
667 Contributes to Disease Progression and Drug Response in Acute Myeloid Leukemia. *Cancer*
668 *Cell* **32**, 324-341 e326 (2017).
669 4. Zeng, Z.*, et al.* Inhibition of CXCR4 with the novel RCP168 peptide overcomes stroma-
670 mediated chemoresistance in chronic and acute leukemias. *Mol Cancer Ther* **5**, 3113-3121
671 (2006).
672 5. Carey, A.*, et al.* Identification of Interleukin-1 by Functional Screening as a Key Mediator of
673 Cellular Expansion and Disease Progression in Acute Myeloid Leukemia. *Cell reports* **18**,
674 3204-3218 (2017).
675 6. Zhang, T.Y.*, et al.* IL-6 blockade reverses bone marrow failure induced by human acute
676 myeloid leukemia. **12**, eaax5104 (2020).
677 7. Wang, B.*, et al.* Exosomes derived from acute myeloid leukemia cells promote
678 chemoresistance by enhancing glycolysis-mediated vascular remodeling. *J Cell Physiol* **234**,
679 10602-10614 (2019).
680 8. Kumar, B.*, et al.* Acute myeloid leukemia transforms the bone marrow niche into a leukemia-
681 permissive microenvironment through exosome secretion. *Leukemia* **32**, 575-587 (2018).
682 9. Hornick, N.I.*, et al.* AML suppresses hematopoiesis by releasing exosomes that contain
683 microRNAs targeting c-MYB. *Science signaling* **9**, ra88 (2016).
684 10. Kouzi, F.*, et al.* Disruption of gap junctions attenuates acute myeloid leukemia
685 chemoresistance induced by bone marrow mesenchymal stromal cells. *Oncogene* **39**, 1198-
686 1212 (2020).
687 11. Omsland, M., Bruserud, Ø., Gjertsen, B.T. & Andresen, V. Tunneling nanotube (TNT)
688 formation is downregulated by cytarabine and NF-κB inhibition in acute myeloid leukemia
689 (AML). *Oncotarget* **8**, 7946-7963 (2017).
690 12. Ye, H.*, et al.* Leukemic Stem Cells Evade Chemotherapy by Metabolic Adaptation to an
691 Adipose Tissue Niche. *Cell Stem Cell* **19**, 23-37 (2016).
692 13. Moschoi, R.*, et al.* Protective mitochondrial transfer from bone marrow stromal cells to
693 acute myeloid leukemic cells during chemotherapy. *Blood* **128**, 253-264 (2016).
694 14. Forte, D.*, et al.* Bone Marrow Mesenchymal Stem Cells Support Acute Myeloid Leukemia
695 Bioenergetics and Enhance Antioxidant Defense and Escape from Chemotherapy. *Cell Metab*
696 **32**, 829-843 e829 (2020).
697 15. Shafat, M.S.*, et al.* Leukemic blasts program bone marrow adipocytes to generate a
698 protumoral microenvironment. *Blood* **129**, 1320-1332 (2017).
699 16. Tabe, Y.*, et al.* Bone Marrow Adipocytes Facilitate Fatty Acid Oxidation Activating AMPK and
700 a Transcriptional Network Supporting Survival of Acute Monocytic Leukemia Cells. *Cancer*
701 *Res* **77**, 1453-1464 (2017).
702 17. Baccelli, I.*, et al.* Mubritinib Targets the Electron Transport Chain Complex I and Reveals the
703 Landscape of OXPHOS Dependency in Acute Myeloid Leukemia. *Cancer Cell* **36**, 84-99.e88
704 (2019).
705 18. Pollyea, D.A.*, et al.* Venetoclax with azacitidine disrupts energy metabolism and targets
706 leukemia stem cells in patients with acute myeloid leukemia. *Nat Med* **24**, 1859-1866 (2018).
707 19. Molina, J.R.*, et al.* An inhibitor of oxidative phosphorylation exploits cancer vulnerability.
708 *Nature Medicine* **24**, 1036-1046 (2018).
709 20. Lagadinou, E.D.*, et al.* BCL-2 inhibition targets oxidative phosphorylation and selectively
710 eradicates quiescent human leukemia stem cells. *Cell Stem Cell* **12**, 329-341 (2013).

711 21. Farge, T.*, et al.* Chemotherapy-Resistant Human Acute Myeloid Leukemia Cells Are Not
712 Enriched for Leukemic Stem Cells but Require Oxidative Metabolism. *Cancer Discov* **7**, 716-
713 735 (2017).
714 22. Li, L.*, et al.* Altered Hematopoietic Cell Gene Expression Precedes Development of Therapy-
715 Related Myelodysplasia/Acute Myeloid Leukemia and Identifies Patients at Risk. *Cancer Cell*
716 **20**, 591-605 (2011).
717 23. Hole, P.S.*, et al.* Overproduction of NOX-derived ROS in AML promotes proliferation and is
718 associated with defective oxidative stress signaling. *Blood* **122**, 3322-3330 (2013).
719 24. Vignon, C.*, et al.* Involvement of GPx-3 in the Reciprocal Control of Redox Metabolism in the
720 Leukemic Niche. *Int J Mol Sci* **21**(2020).
721 25. Itoh, K.*, et al.* Reproducible establishment of hemopoietic supportive stromal cell lines from
722 murine bone marrow. *Exp Hematol* **17**, 145-153 (1989).
723 26. Childress, C.C., Sacktor, B. & Traynor, D.R. Function of carnitine in the fatty acid oxidase-
724 deficient insect flight muscle. *J Biol Chem* **242**, 754-760 (1967).
725 27. Stephens, F.B., Constantin-Teodosiu, D. & Greenhaff, P.L. New insights concerning the role of
726 carnitine in the regulation of fuel metabolism in skeletal muscle. *J Physiol* **581**, 431-444
727 (2007).
728 28. Liu, X.*, et al.* Acetate Production from Glucose and Coupling to Mitochondrial Metabolism in
729 Mammals. *Cell* **175**, 502-513 e513 (2018).
730 29. Vysochan, A., Sengupta, A., Weljie, A.M., Alwine, J.C. & Yu, Y. ACSS2-mediated acetyl-CoA
731 synthesis from acetate is necessary for human cytomegalovirus infection. *Proc Natl Acad Sci*
732 *U S A* **114**, E1528-E1535 (2017).
733 30. Tiziani, S.*, et al.* Metabolomic profiling of drug responses in acute myeloid leukaemia cell
734 lines. *PLoS One* **4**, e4251 (2009).
735 31. Nogueira-Pedro, A.*, et al.* Hydrogen peroxide (H2O2) induces leukemic but not normal
736 hematopoietic cell death in a dose-dependent manner. *Cancer Cell International* **13**, 123
737 (2013).
738 32. Taniguchi Ishikawa, E.*, et al.* Connexin-43 prevents hematopoietic stem cell senescence
739 through transfer of reactive oxygen species to bone marrow stromal cells. *Proc Natl Acad Sci*
740 *U S A* **109**, 9071-9076 (2012).
741 33. Davidson, J.S., Baumgarten, I.M. & Harley, E.H. Reversible inhibition of intercellular
742 junctional communication by glycyrrhetinic acid. *Biochem Biophys Res Commun* **134**, 29-36
743 (1986).
744 34. Davidson, J.S. & Baumgarten, I.M. Glycyrrhetinic acid derivatives: a novel class of inhibitors
745 of gap-junctional intercellular communication. Structure-activity relationships. *J Pharmacol*
746 *Exp Ther* **246**, 1104-1107 (1988).
747 35. Lyssiotis, C.A. & Cantley, L.C. Acetate fuels the cancer engine. *Cell* **159**, 1492-1494 (2014).
748 36. Comerford, S.A.*, et al.* Acetate dependence of tumors. *Cell* **159**, 1591-1602 (2014).
749 37. Gao, X.*, et al.* Acetate functions as an epigenetic metabolite to promote lipid synthesis under
750 hypoxia. *Nat Commun* **7**, 11960 (2016).
751 38. Schug, Z.T.*, et al.* Acetyl-CoA synthetase 2 promotes acetate utilization and maintains cancer
752 cell growth under metabolic stress. *Cancer Cell* **27**, 57-71 (2015).
753 39. Yoshii, Y.*, et al.* Cytosolic acetyl-CoA synthetase affected tumor cell survival under hypoxia:
754 the possible function in tumor acetyl-CoA/acetate metabolism. *Cancer Sci* **100**, 821-827
755 (2009).
756 40. Sousa, C.M.*, et al.* Pancreatic stellate cells support tumour metabolism through autophagic
757 alanine secretion. *Nature* **536**, 479-483 (2016).
758 41. Sonveaux, P.*, et al.* Targeting lactate-fueled respiration selectively kills hypoxic tumor cells in
759 mice. *J Clin Invest* **118**, 3930-3942 (2008).

760 42. Whitaker-Menezes, D.*, et al.* Evidence for a stromal-epithelial "lactate shuttle" in human
761 tumors: MCT4 is a marker of oxidative stress in cancer-associated fibroblasts. *Cell Cycle* **10**,
762 1772-1783 (2011).
763 43. Saborano, R.*, et al.* A framework for tracer-based metabolism in mammalian cells by NMR.
764 *Sci Rep* **9**, 2520 (2019).
765 44. Mashimo, T.*, et al.* Acetate is a bioenergetic substrate for human glioblastoma and brain
766 metastases. *Cell* **159**, 1603-1614 (2014).
767 45. Testa, U., Labbaye, C., Castelli, G. & Pelosi, E. Oxidative stress and hypoxia in normal and
768 leukemic stem cells. *Experimental Hematology* **44**, 540-560 (2016).
769 46. Kocabas, F.*, et al.* Hypoxic metabolism in human hematopoietic stem cells. *Cell & bioscience*
770 **5**, 39 (2015).
771 47. Takubo, K.*, et al.* Regulation of glycolysis by Pdk functions as a metabolic checkpoint for cell
772 cycle quiescence in hematopoietic stem cells. *Cell Stem Cell* **12**, 49-61 (2013).
773 48. Shan, T.*, et al.* Cancer-associated fibroblasts enhance pancreatic cancer cell invasion by
774 remodeling the metabolic conversion mechanism. *Oncol Rep* **37**, 1971-1979 (2017).
775 49. Migneco, G.*, et al.* Glycolytic cancer associated fibroblasts promote breast cancer tumor
776 growth, without a measurable increase in angiogenesis: evidence for stromal-epithelial
777 metabolic coupling. *Cell Cycle* **9**, 2412-2422 (2010).
778 50. Pavlides, S.*, et al.* The reverse Warburg effect: aerobic glycolysis in cancer associated
779 fibroblasts and the tumor stroma. *Cell Cycle* **8**, 3984-4001 (2009).
780 51. Cruz-Bermudez, A.*, et al.* Cancer-associated fibroblasts modify lung cancer metabolism
781 involving ROS and TGF-beta signaling. *Free Radic Biol Med* **130**, 163-173 (2019).
782 52. Hole, P.S.*, et al.* Overproduction of NOX-derived ROS in AML promotes proliferation and is
783 associated with defective oxidative stress signaling. *Blood* **122**, 3322-3330 (2013).
784 53. Robinson, A.J.*, et al.* Reactive Oxygen Species Drive Proliferation in Acute Myeloid Leukemia
785 via the Glycolytic Regulator PFKFB3. *Cancer Res* **80**, 937-949 (2020).
786 54. Arranz, L.*, et al.* Neuropathy of haematopoietic stem cell niche is essential for
787 myeloproliferative neoplasms. *Nature* **512**, 78-81 (2014).
788 55. Corral, J.*, et al.* An Mll-AF9 fusion gene made by homologous recombination causes acute
789 leukemia in chimeric mice: a method to create fusion oncogenes. *Cell* **85**, 853-861 (1996).
790 56. Ludwig, C. & Gunther, U.L. MetaboLab--advanced NMR data processing and analysis for
791 metabolomics. *BMC Bioinformatics* **12**, 366 (2011).
792 57. Reed, M.A.C., Roberts, J., Gierth, P., Kupce, E. & Gunther, U.L. Quantitative Isotopomer Rates
793 in Real-Time Metabolism of Cells Determined by NMR Methods. *Chembiochem* **20**, 2207-
794 2211 (2019).

795

796

797

798 **EXTENDED DATA: Crosstalk between AML and stromal cells triggers**
799 **acetate secretion through the metabolic rewiring of stromal cells**

800 Nuria Vilaplana-Lopera[1], Ruba Almaghrabi[1*], Grigorios Papatzikas[1*], Vincent Cuminetti[2*], Mark
801 Jeeves[1], Elena González[1], Alan Cunningham[3], Ayşegül Erdem[3], Frank Schnuetgen[4,5,6], Manoj
802 Raghavan[1,7], Sandeep Potluri[1,7], Jean-Baptiste Cazier[1], Jan Jacob Schuringa[3], Michelle AC Reed[1],
803 Lorena Arranz[2], Ulrich L Günther[1,8†] and Paloma Garcia[1,9†],

804 [1] Institute of Cancer and Genomic Sciences, University of Birmingham, Birmingham B15 2TT, United Kingdom
805 [2] Stem Cells, Ageing and Cancer Research Group, Department of Medical Biology, Faculty of Health Sciences, UiT – The
806 Arctic University of Norway, 9019 Tromsø, Norway
807 [3] Department of Experimental Hematology, University Medical Center Groningen, University of Groningen, Hanzeplein 1,
808 9700 RB, Groningen, The Netherlands.
809 [4] Department of Medicine, Hematology/Oncology, University Hospital Frankfurt, Goethe-University, 60590 Frankfurt,
810 Germany.
811 [5] Frankfurt Cancer Institute, Goethe-University Frankfurt, 60596 Frankfurt, Germany.
812 [6] German Cancer Consortium (DKTK), partner site Frankfurt/Mainz, and German Cancer Research Center (DKFZ),
813 Heidelberg, Germany
814 [7] Centre for Clinical Haematology, University Hospitals Birmingham NHS Foundation Trust, Queen Elizabeth Hospital,
815 Queen Elizabeth Medical Centre, Birmingham, United Kingdom.
816 [8] Institute of Chemistry and Metabolomics, University of Lübeck, 23562 Lübeck, Germany
817 [9] Corresponding author
818 [*] These authors contributed equally
819 [†] These two authors are co-senior authors.

820

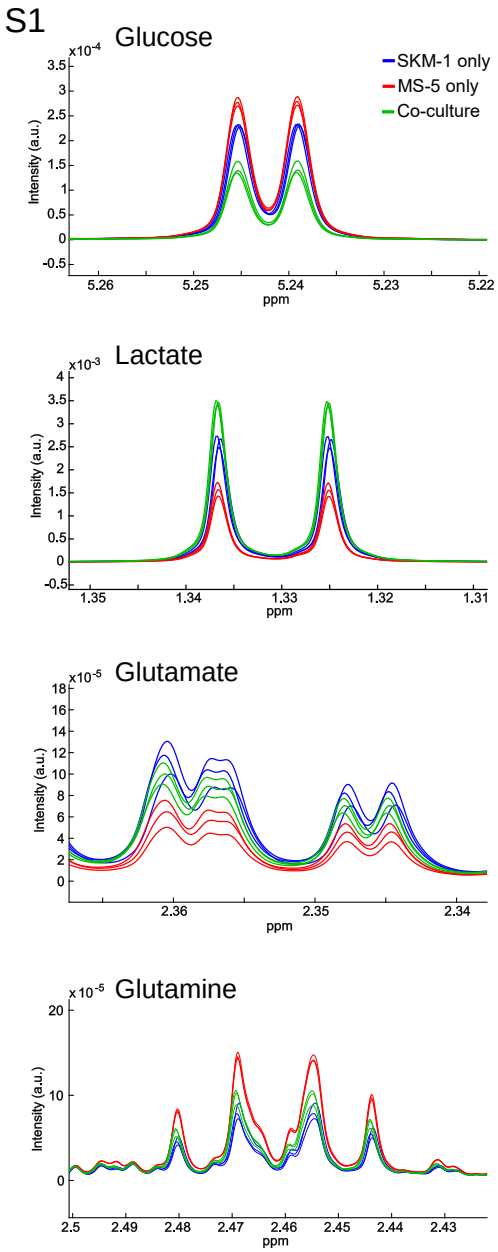

Extended Data Figure 1. Other extracellular metabolite levels in co-cultures with SKM-1 and MS-5 cells

Sections of ^{1}H-NMR spectra from extracellular medium samples of SKM-1 cells cultured alone (blue), MS-5 cells cultured alone (red) and SKM-1 and MS-5 cells in co-culture (green) after 24 hours of culture, corresponding to glucose, lactate, glutamate and glutamine.

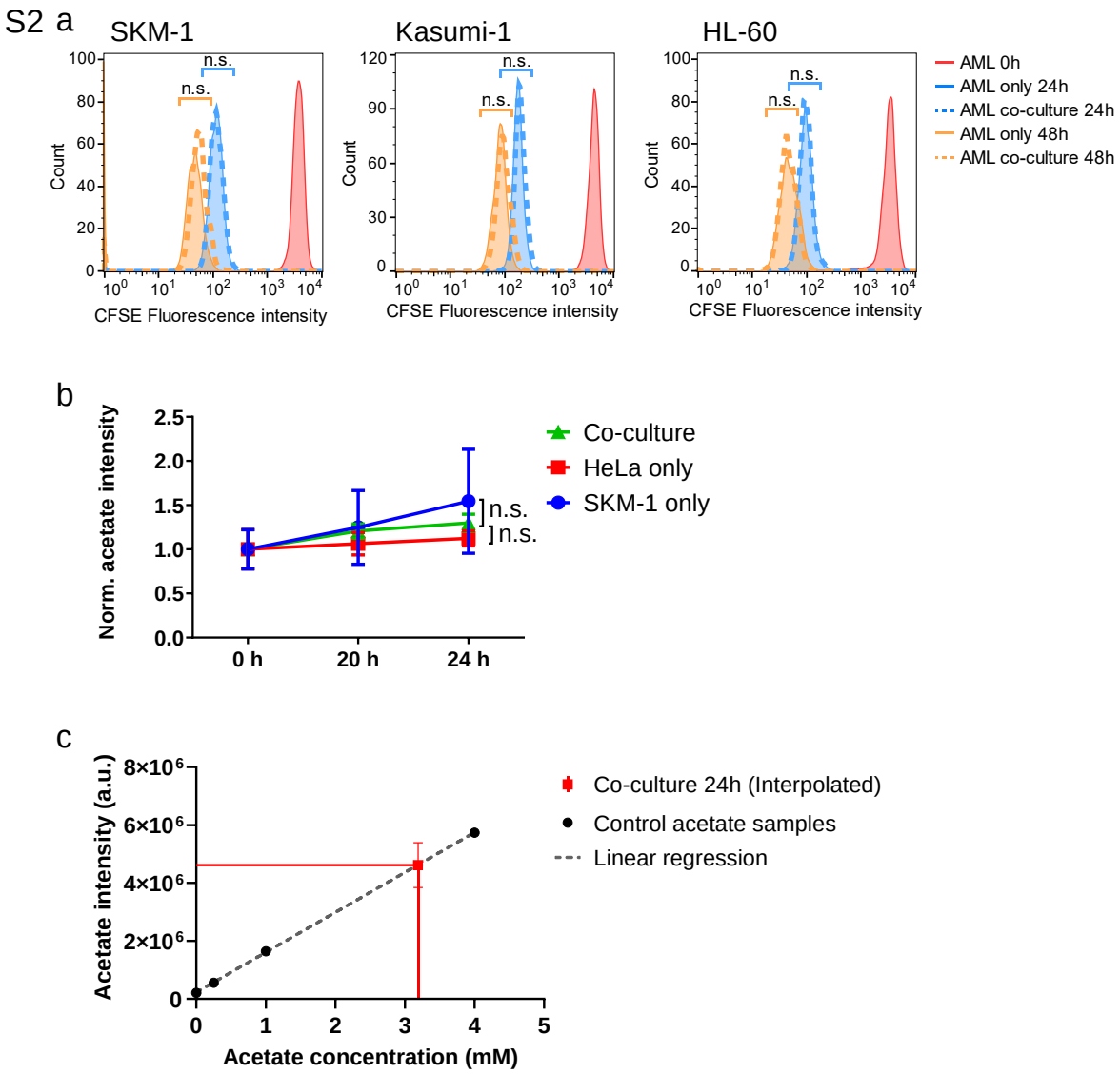

Extended Data Figure 2. Proliferation in co-culture, co-culturing AML cells with an unrelated cell line (HeLa) and titration of acetate concentration in co-culture

A) CFSE cell proliferation analysis in AML cell lines alone or in co-culture with MS-5 cells. The population of living cells was gated, and 1500 cells for each condition were randomly selected and plotted. The geometric mean for each population and time point was compared between cells alone or in co-culture by performing an unpaired unpaired Student's t-test and p-values were represented as n.s. for not significant. Each histogram is representative of n=3 independent experiments.

B) Extracellular acetate levels in SKM-1 cells cultured alone (blue), HeLa cells cultured alone (red) and AML and HeLa cells in co-culture (green) at 0, 20 and 24 hours. Each point represents the mean of n=3 independent experiments and error bars represent standard deviation. An

839 unpaired Student's t-test was applied for each condition (black brackets) and p-values are
840 represented by n.s. for not significant.

841 C) Linear regression of acetate concentrations and detected intensities in ^{1}H-NMR spectra
842 (Intensity=$1.38 \cdot 10^{6} \pm 1.6 \cdot 10^{4}$ x Acetate concentration + $2.27 \cdot 10^{5} \pm 3.3 \cdot 10^{4}$; R^{2}=0.9987). The
843 intensities detected in samples of co-culture were interpolated to obtain the estimate acetate
844 concentration in co-culture (3.09 mM). Each point represents the mean of n=3 independent
845 experiments and error bars represent standard deviation.

846

S3

a

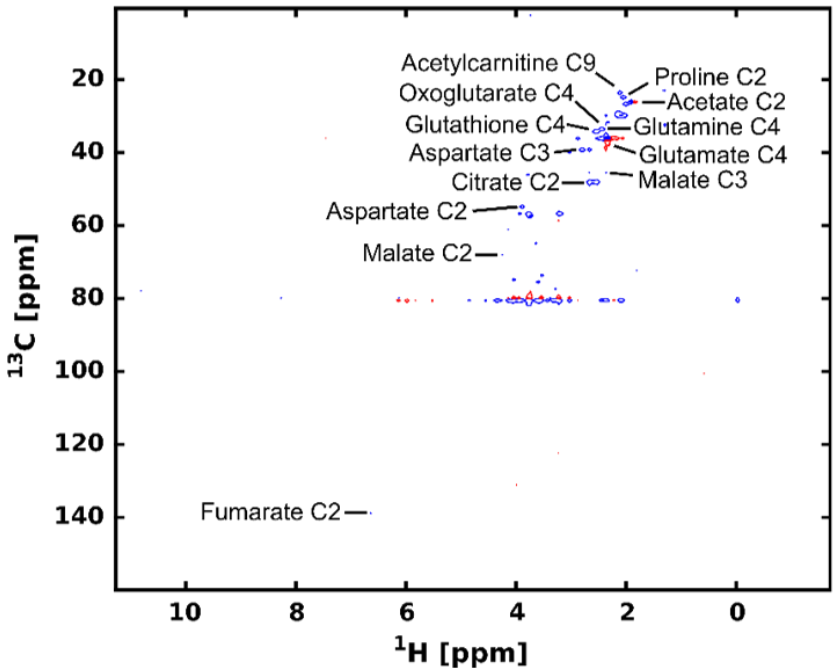

b

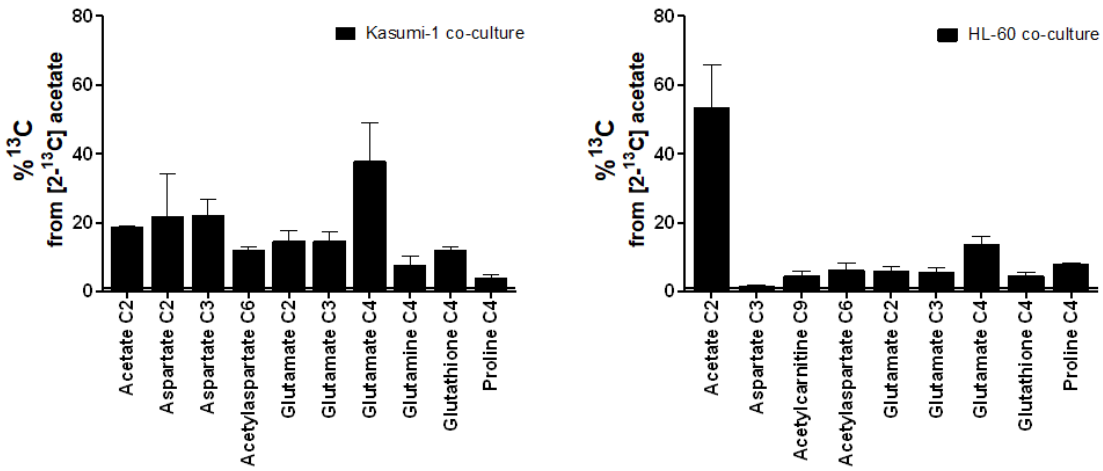

847

848 **Extended Data Figure 3. Label incorporation from [2-^{13}C]acetate in SKM-1 and MS-5 cells**
849 **cultured alone**

850 A) Example of metabolites assigned in a ^{1}H-^{13}C-HSQC spectrum from a polar extract from SKM-1
851 cells cultured with [2-^{13}C]acetate for 2 hours. ^{13}C percentages were calculated in 13 carbons
852 from 11 different metabolites. The exact chemical shifts for each carbon are: acetate C2, 1.91
853 ppm (^{1}H) – 26.1 ppm (^{13}C); aspartate C2, 3.89 ppm (^{1}H) – 55.0 ppm (^{13}C); aspartate C3, 2.82 ppm
854 (^{1}H) – 39.4 ppm (^{13}C); acetylcarnitine C9, 2.15 ppm (^{1}H) – 23.4 ppm (^{13}C); citrate C2, 2.52 ppm

855 (^{1}H) – 48.2 ppm (^{13}C); fumarate C2, 6.51 ppm (^{1}H) – 138.2 ppm (^{13}C); glutamate C4, 2.34 ppm (^{1}H)
856 – 36.1 ppm (^{13}C); glutamine C4, 2.44 ppm (^{1}H) –33.7 ppm (^{13}C); oxoglutarate C4, 2.43 ppm (^{1}H) –
857 33.4 ppm (^{13}C); glutathione C4, 2.55 ppm (^{1}H) – 34.2 ppm (^{13}C); malate C2, 4.28 ppm (^{1}H) – 73.2
858 ppm (^{13}C); malate C3, 2.68 ppm (^{1}H) – 45.4 ppm (^{13}C); and proline C4, 2 ppm (^{1}H) – 26.6 ppm
859 (^{13}C).

860 B) ^{13}C percentages on polar metabolites in Kasumi-1 and HL-60 cells in co-culture with MS-5 cells.
861 Cells were co-cultured for 24 hours before the addition of extra 4 mM sodium [2-^{13}C]acetate.
862 Bars represent the mean of the ^{13}C percentage and error bars represent the standard deviation
863 of n=3 independent experiments.
864 ^{13}C natural abundance is represented as a black bar at %^{13}C = 1.1.

865

S4 a

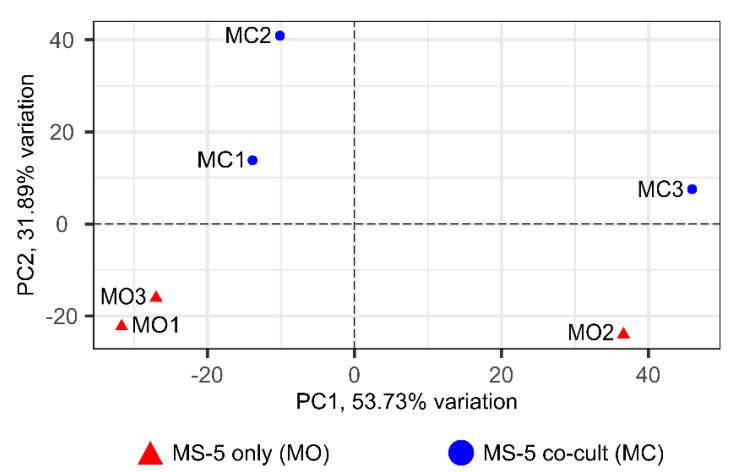
MC2
MC1
MC3
MO3
MO1
MO2
PC2, 31.89% variation
PC1, 53.73% variation
40
20
0
-20
-20
0
20
40
MS-5 only (MO)
MS-5 co-cult (MC)

b

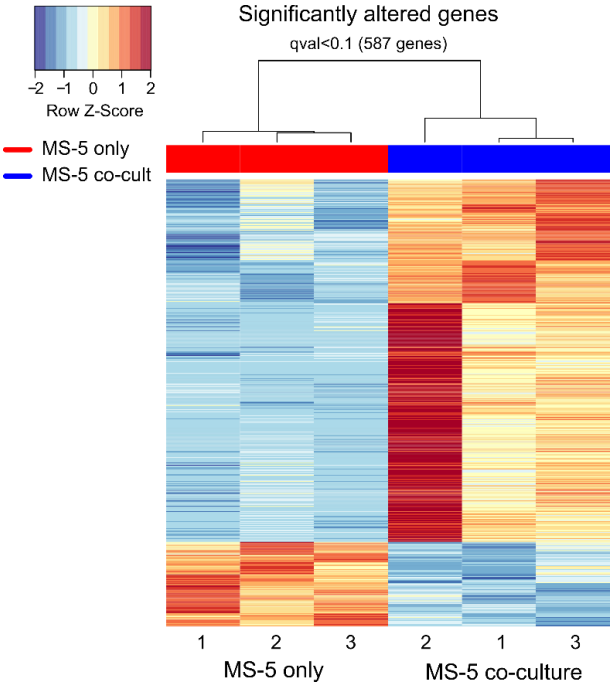
Significantly altered genes
qval<0.1 (587 genes)
−2 −1 0 1 2
Row Z-Score
MS-5 only
MS-5 co-cult
1 2 3 2 1 3
MS-5 only
MS-5 co-culture

c

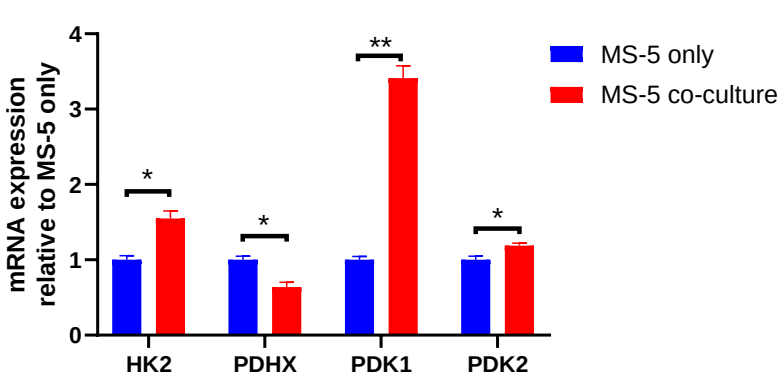
mRNA expression relative to MS-5 only
0
1
2
3
4
*
*
**
*
HK2
PDHX
PDK1
PDK2
MS-5 only
MS-5 co-culture

866

867 **Extended Data Figure 4. PCA component analysis, heat map of differentially expressed**
868 **genes and qPCR for MS-5 cells cultured alone and in co-culture with SKM-1 cells**

869 A) PCA plot showing the clustering of individual samples of MS-5 cells cultured alone (MO) and MS-
870 5 cells in co-culture (MC). The x and y axis values represent the variation between the sample
871 groups. Generated using Sleuth 0.30.0 R statistical package.
872 B) Heat map of differentially expressed genes in MS-5 only (red) vs MS-5 co-culture (blue)
873 calculated using the Wald statistical test, correcting for multiple testing comparison employing
874 the Benjamini-Hochberg method using a false discovery rate threshold of 1% (q-value<0.01).
875 Generated using Sleuth 0.30.0 R statistical package.
876 C) Quantitative PCR mRNA expression values for RNA sequencing validation of MS-5 cells cultured
877 alone and in co-culture with SKM-1 cells. The gene set chosen was *Hk2*, *Pdhx*, *Pdk1* and *Pdk2*.
878 mRNA quantification was normalized to *B2m* house-keeping gene. Bars represent the mean and
879 error bars represent the SEM of three independent experiments. An unpaired Student's t-test
880 was applied for each gene and p-values are represented by * for p-value<0.05, ** for p-
881 value<0.01 and *** for p-value<0.001.

882

S5

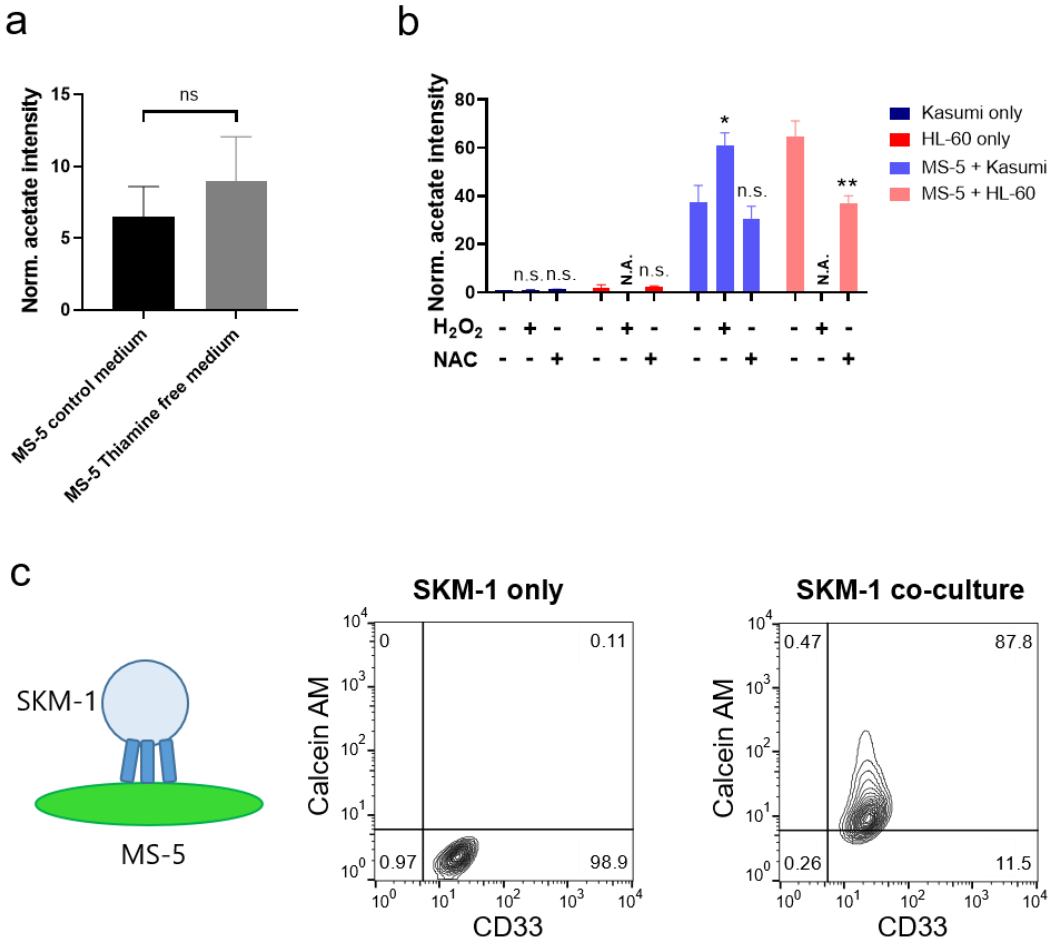

883

884 **Extended Data Figure 5. Acetate secretion in thiamine free medium and after modulating**
885 **ROS levels and calcein-AM transfer through GAP junctions in AML-stromal co-cultures**

886 A) Extracellular acetate levels in MS-5 cells cultured in control medium (black) or in thiamine-
887 depleted medium (grey) after 24 hours.
888 B) Extracellular acetate levels in Kasumi (navy blue) and HL-60 (red) cultured alone and in co-
889 culture (light blue and light red) for 24 hours in a control medium, medium with 50 µM H_2O_2
890 or medium with 5 mM NAC. Acetate levels for HL-60 cells cultured alone or under co-culture
891 with 50 µM H_2O_2 are not shown as treatment 50 µM H_2O_2 severely impaired their viability.
892 N.A. = not analysed.
893 For A and B each point represents the mean of n=3 independent experiments and error bars
894 represent standard deviation. An unpaired Student's t-test was applied for each condition
895 (black brackets) and p-values are represented by n.s. for not significant. * for p-value<0.05
896 and ** for p-value<0.01.

897 C) Representative flow cytometry diagrams showing CD33 and calcein-AM green fluorescence
898 in SKM-1 cells cultured alone or SKM-1 cells in co-culture with Calcein-AM-stained MS-5 cells
899 after 3 hours. Frequencies of gated cell populations are indicated.
900

901 **Extended Data Table 1. Primary AML samples' additional information**

Samples obtained from Martini Hospital, UMCG

Patient	Tissue of origin	Type of AML (FAB)	Karyotype	Other mutations	Risk
AML1	PB	M5	Normal	FLT3-ITD; NPM1; DNMTA3; IDH2	Adv
AML2	PB	M1	Unknown	-	Adv

902

Samples obtained from University Hospital Birmingham NHS Foundation Trust, UoB

Patient	Tissue of origin	Type of disease	Karyotype	Other mutations
AML3	PB	Secondary AML from MDS	46,XY	TET2; SRSF2; RUNX1; CEBPA; ASXL1
AML4	PB	Secondary AML from MDS	46,XY	NPM1 neg FLT3 neg
AML5	PB	AML M1 (FAB)	46 XX	FLT3-ITD, 2xWT1, CEBPA
AML6	PB	AML M2 (FAB)	46 XX	-
AML7	PB	AML M4 (FAB)	46 XY	-

903